Measurement of air temperature and humidity in harsh environment

MASTER'S THESIS

submitted in partial fulfillment of the requirements for the degree of

Diplom-Ingenieur

in

Electrical Engineering

by

Flatscher Matthias

Registration Number 0831505

to the Faculty of Electrical and Information Engineering
at the Graz University of Technology

Advisor: Univ.-Prof. Dipl.-Ing. Dr. techn. Hubert Zangl
Assistance: Dipl.-Ing. Dr. techn. Thomas Bretterklieber
                  Dipl.-Ing. Dr. techn. Markus Neumayer
                  Dipl.-Ing. Dr. techn. Moser Michael

Graz, 13.10.2014   _____   _____
                                          (Signature of Author)   (Signature of Advisor)

Statutory Declaration

Flatscher Matthias
Grazbachgasse 44, 8010 Graz

I declare that I have authored this thesis independently, that I have not used other than the declared sources / resources and that I have explicitly marked all material which has been quoted either literally or by content from the used sources.

Graz, 13.10.2014

(Place, Date)

(Signature Flatscher Matthias)

Acknowledgements

Abstract

This thesis presents the development and construction of a weather and radiation shield. The construction is used to ensure the measurement of air temperature and humidity in harsh environment. Therefore the influence of ice and snow should be minimized. A heating device achieves that the housing is partial free of ice and snow.

The thesis starts with a system concept including the mechanical layout of the weather and radiation shield. The following design of the heating unit is based on the geometry of the housing. To estimate the needed heating power analytical calculations and *CFD* simulations are made. To keep the power consumption low an ice detection unit is realized as well.

The realized system is tested in a climate cabinet. It is shown that it is possible to get rid of an ice layer. Furthermore the meteorological temperature is just minimally distorted by the heating process. It also has been shown that the ice detection unit is capable to detect the presence of an ice layer.

Kurzfassung

Die vorliegende Arbeit beschreibt die Entwicklung und Konstruktion eines Wetter- und Sonnenstrahlungsschutzes. Dieser soll die Messung von Lufttemperatur und Feuchtigkeit auch unter widrigsten Umständen gewährleisten. Hierbei wird versucht den Einfluss von Eis und Schnee zu minimieren. Dafür wird das Gehäuse partiell beheizt.

Die Arbeit beginnt mit dem mechanischen Entwurf eines Wetter- und Strahlungsschutzes. Aufbauend auf dessen Geometrie wird die Heizvorrichtung entworfen. Um die benötigte Heizleistung abzuschätzen werden neben analytischen Berechnungen auch *CFD* Simulationen durchgeführt. Mit Hilfe eines Eisdetektors soll die Heizleistung optimiert werden.

Das realisierte System wurde in einem Klimaschrank vermessen. Mit Hilfe der Messungen wird gezeigt, dass es möglich ist Eis abzutauen. Zudem wird gezeigt dass durch den Heizvorgang die meteorologische Temperaturmessung nur minimal verfälscht wird. Der entworfene Eisdetektor ist in der Lage, eine etwaige Eisanlagerung zu erkennen.

Contents

CHAPTER 1

Introduction

1.1 Motivation

Measurements of air temperature and humidity depend on a variety of influencing factors. To measure meteorological data environmental impacts must be considered as well as how they effect the measurement instrument. For example, if sun radiation heats up a solid state sensor, this leads to wrong measurement results. Therefore it is necessary to produce devices which provide accurate results e.g. by using sensors which are surrounded by a weather and radiation shield. Thus sensors can be also affected by weather aspects which are not the target of the measurement. Ice and snow are main problems because moveable parts are not longer able to work as can be seen in figure 1.1. The air circulation could be disturbed in an ice and snow covered weather and radiation shield (figure 1.2). This thesis shows the development and construction of a weather and radiation shield which should be capable to deliver reliable measurement data under such rough conditions.

Figure 1.1: Disturbed movement of a cup anemometer and wind vane caused by ice and snow [1].

Figure 1.2: Ice covered housing of a rain collector [2].

1.2 State of the art

There are a couple of ways how to measure the air temperature and humidity. For this research the main aspect is how this devices are protected against icing. Table 1.1 shows a rough comparison between a couple of devices.

The solution of *Galltec Mess- und Regelungstechnik GmbH* uses a non ventilated weather and radiation shield and has no gadget against icing. It is the simplest design of the listed realisations and therefore, with and without sensor, the cheapest device.

Rotronic AG offers a ventilated weather and radiation shield which achieves, in combination with a sensor from *Rotronic AG*, practically identical values as a dew point mirror measurement [3]. A fan supplies the sensor with fresh air even when the environment is windless. Therefore in the housing occurs no micro-climate. This device has also no gadget that protects against icing.

The only device with a weather and radiation shield in table 1.1, including a gadget against icing is offered by *Meteo Labor AG*. This device uses a partial heated weather and radiation shield with two heating resistors in the roof and also a ventilator which heats the air. The system uses a dew point mirror hygrometer. The relative air humidity is determined with the measured dew point, in combination with the air temperature and a control unit. The humidity accuracy is not specified [4].

An other method to measure the air temperature is the speed of sound. The propagation of sound depends highly on the air temperature, but is hardly affected by air pressure and humidity. This kind of instrument measures the virtual temperature which is referred to dry air (0 % humidity) and the same pressure like the actual measured value. This measurement neglects the air humidity. At a air temperature of 20 °C and a relative humidity of 100 % the virtual temperature is approximately 2 K too high. If the absolute humidity a is known, the difference between the measured virtual temperature T_v and the real air temperature T_r can be approximately corrected with equation 1.1 [5].

$$T_\mathrm{r} = T_\mathrm{v} - 0.135 \; \frac{\mathrm{K \; m^3}}{\mathrm{g}} \cdot a \qquad (1.1)$$

After respective correction of the humidity influence the procedure exceeds the accuracy of the classic procedures of the temperature measurement in a weather and thermal radiation shield [6].

The advantage of variables measured by the speed of sound is, on the one hand its inertia free reaction to the actual gas temperature, and on the other hand the avoidance of measurement errors such as those which occur when a solid state temperature sensor is heated up by radiation [7].

An other advantage is that the measurement heads can be heated. Therefore such devices are the only solution which offers a complete ice protection. By using heating elements this device needs more power. For example the anemometer from *Thies* in table 1.1 needs 90 VA with heating and 2.5 VA without.

The measurement of temperature via the speed of sound is currently not accredited according to the internationally valid MEASNET regulations (`www.measnet.com`).

A disadvantage is that this method neglects the air humidity. Thus the speed of sound can just be used to determine the temperature. Therefore an additional sensor is needed to measure the humidity which has to be protected against icing as well.

There are also weather stations available which measure and record wind speed and direction, air temperature and relative humidity, barometric pressure and solar radiation, rain- and snowfall. But also such a weather station like one from *WeatherHawk* does not use the possibility to measure the air temperature with ultrasonic instead it is measured with a NTC - resistor.

Manufacturer	Housing	Temperature measurement principle and accuracy	Humidity measurement principle and accuracy	Price and model / order number
Galltec Mess- und Regelung- stechnik GmbH	Passive weather and radiation shield	PT100 - 1/3 DIN ± 0.2 K additional error: ±0.004 %/K for < 10 °C, > 40 °C	Capacitive for 5 ... 95%rH at 10 ... 40 °C ± 0.2%rH additional error: < 0.1 %/K for < 10 °C, > 40 °C %rH	Sensor (P6312 [8]): € 467[1] excl. VAT Housing (P6300 [8]): € 196[1] excl. VAT
Rotrinic AG	Ventilated weather and radiation shield aspiration rate: 3.5 m/s respectively 900 l/min	± 0.1 K @ 23 °C	±0.8 %rH @ 23 °C	Sensor (MP102H-A10300 [9]): € 615[2] Housing (RS12T / RS24T [10]): € 830[2]
Meteo Labor AG	Partially heated and ventilated weather and radiation shield	copper - constantan ± 0.15 K for range -20 °C to +50 °C ± 0.25 K for range -65 °C to -50 °C	dew point mirror hygrometer accuracy is not specified	€ 9666[3] excl. VAT (VTP 37-RS232 [4])
Adolf Thies GmbH & Co. KG	Sensors and instrument body are automatically heated	Speed of sound ±0.5 K to 35 $\frac{m}{s}$	———————	€ 2797[1] excl. VAT (P6003H [7])
WeatherHawk	Ventilated weather and radiation shield	NTC - resistor ± 0.2 K for range -20 °C to 50 °C ± 0.5 K for range < -20 °C and > 50 °C	Capacitive ± 2 %rH	$ 6379[4] (Model-611 [11])

Table 1.1: Comparison between different solutions

[1] offer by: www.ammonit.com
[2] offer by: www.rotronic.com
[3] offer by: www.meteolabor.ch
[4] direct available at www.weatherhawk.com/611-series

Proposed system concept

This thesis uses the approach of a weather and radiation shield. The prototype is constructed of acrylic glass. The housing is depicted in figure 2.1 and has a high of 300 mm and a diameter of 150 mm. To keep the weather and radiation shield partial free from ice a heating unit is used. This heating unit has four holes and is mounted on the bottom side of the housing. To guarantee the ventilation of the housing small fans are attached to the holes. In figure 2.1 one fan is displayed. They are used to blow out the fluid. To avoid a distortion of the temperature by the movement of the fans just two fans are turned on at the same time. Thus the surrounding air is sucked in through the wholes of the still standing fans. The heating process and the fans are controlled by the CONTROL - PCB which is placed in the upper chamber of the housing.

An additional cylinder (h = 110 mm, $\varnothing_{out}$ = 110 mm, $\varnothing_{in}$ = 104 mm) is placed in the lower chamber. This cylinder should avoid additional turbulence and the movement of the cables. The cables connect the CONTROL - PCB with the heating unit and the STACK - PCB which lays on top of it.

The STACK - PCB includes among others the fan sockets and the necessary electronic to turn them on and off. The meteorological sensor takes place in the lower chamber. It is placed at the bottom of another cylinder (h = 155 mm, $\varnothing_{out}$ = 20 mm, $\varnothing_{in}$ = 14 mm) which is fixed by a shaft bracket in the top chamber.
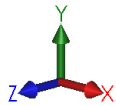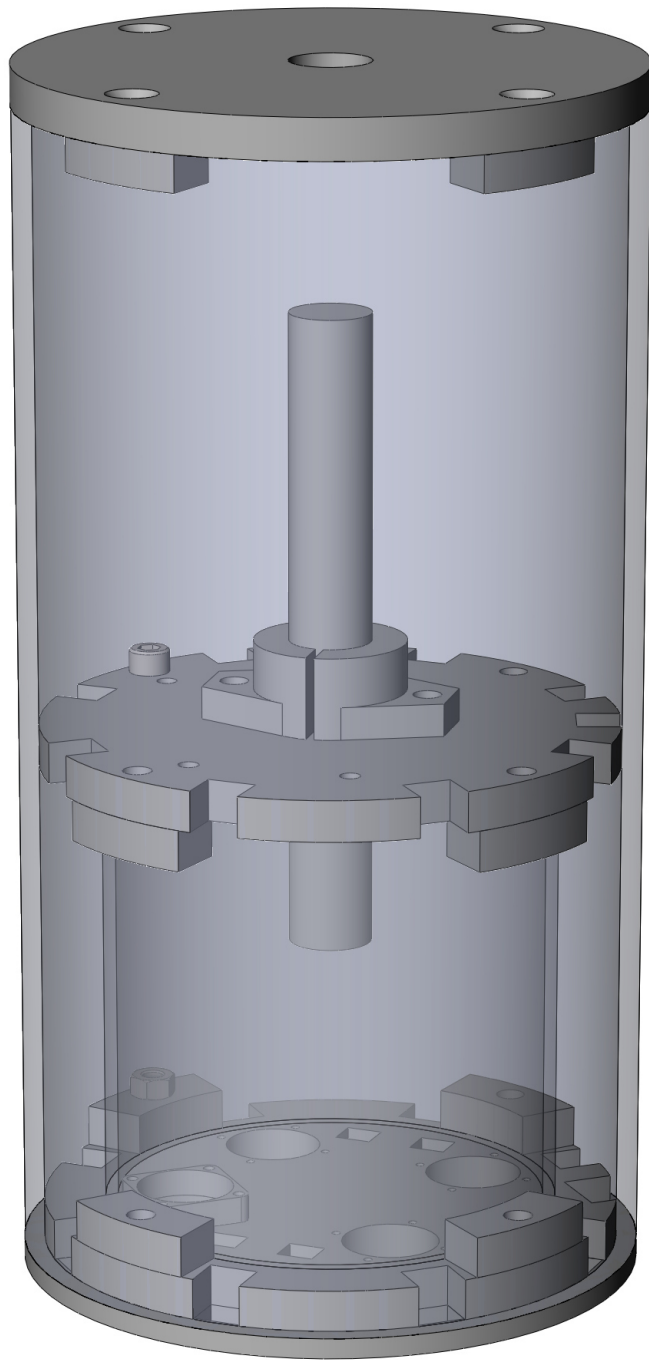
Figure 2.1: Weather and radiation shield with a heated bottom surface. At the bottom of the small cylinder, in the middle of the housing, the meteorological sensor is placed.

Heating unit

In this section the design of the heating unit and which power is needed to hold its surface above 0 °C is discussed.

3.1   Layout and electrical calculations

The heating unit is an ordinary copper coil which is realized as a PCB. A quarter of the implementation, which consists of two segments, is depicted in figure 3.1. The dimensions of the heating unit are

$$d_{\text{Heater}} \; = \; 0.15 \text{ m} \qquad w_{\text{Cu}} \; = \; 150 \; \mu\text{m} \qquad w_{\text{PCB}} \; = \; 150 \; \mu\text{m} \qquad h_{\text{Cu}} \; = \; 35 \; \mu\text{m}.$$

The diameter of the heating unit is d_{Heater}, w_{Cu} is the width of the circuit path and h_{Cu} the high, w_{PCB} is the distance between the circuit path itself. The heating unit is designed with *EAGLE*, therefore a ULP (User Language Program) is written. To keep the resistance low and therefore the needed voltage to keep the surface above 0 °C the heating unit is split up into eight segments. Four wholes with a diameter $d_{\text{ventilation}}$ of 23.5 mm are used for the ventilation of the weather and radiation shield.
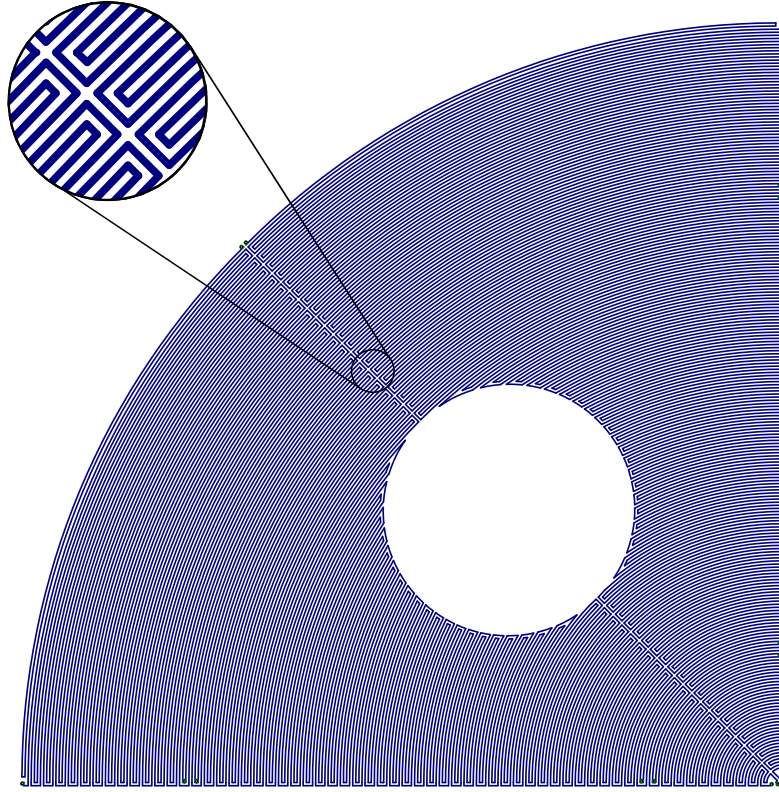
Figure 3.1: A quarter of the heating unit with one ventilation hole.

The length l of each segment can be obtained in *EAGLE*. The resistance R_segment of one heating segment at a temperature of 0 °C can be calculated with the following formula. The specific electrical resistance for copper ρ_Cu at a temperature of 0 °C is taken from [12, page 237].

$$R \;=\; \frac{\rho_\text{Cu} \cdot l}{A_\text{Profile}} \;=\; \frac{\rho_\text{Cu} \cdot l}{w_\text{Cu} \cdot h_\text{Cu}} \tag{3.1}$$

$$R_\text{segment} \;=\; \frac{0.0156 \cdot 10^{-6} \; \frac{\Omega \cdot \text{m}^2}{\text{m}} \cdot 6.4835 \; \text{m}}{0.15 \cdot 10^{-3} \; \text{m} \cdot 0.035 \cdot 10^{-3} \; \text{m}} \;=\; 19.2653 \; \Omega$$

Therefore the power dissipation of one segment is

$$P_\text{segment} \;=\; \frac{V^2}{R_\text{segment}},$$

and for the whole heating unit

$$P \;=\; P_\text{segment} \cdot 8.$$

The thermal energy Q produced by the whole heating unit is

$$Q \;=\; P \cdot t \;=\; \alpha \cdot A_{\text{Heater}} \cdot t \cdot \Delta\, T \;=\; \alpha \cdot A_{\text{Heater}} \cdot t \cdot \left(T_{\text{Heater}} \cdot T_{\text{Fluid}}\right). \qquad (3.2)$$

The surface temperature of the heating unit is T_{Heater}, T_{Fluid} is the temperature of the surrounding medium, A_{Heater} is the area of the heating unit, α is the heat transfer coefficient of the surrounding medium and t the time.

3.2   Thermal calculations

To evaluate the needed power to keep the temperature of the heating unit at a certain level we have to determine the missing quantities in formula 3.3.

$$P \;=\; \alpha \cdot A_{\text{Heater}} \cdot \left(T_{\text{Heater}} \;-\; T_{\text{Fluid}}\right). \qquad (3.3)$$

$$P \;=\; \alpha \cdot \left(r^2_{\text{Heater}} \cdot \pi \;-\; 4 \cdot r^2_{\text{ventilation}} \cdot \pi\right) \cdot \left(T_{\text{Heater}} \;-\; T_{\text{Fluid}}\right)$$

We have to do that for two cases, the forced and the free convection.

To calculate the heat transfer coefficient α the quantities from table 3.1 are needed.

Name	Symbol	Unit
heat conductivity	λ	$\frac{\text{W}}{\text{m}\cdot\text{K}}$
kinematic viscosity	ν	$\frac{\text{m}^2}{\text{s}}$
Prandtl number	Pr	—
Nusselt number	Nu	—
Reynolds number	Re	—

Table 3.1: Thermodynamic quantities

The values for λ, ν and Pr, are taken from *VDI - Wärmeatlas* [13, page Dbb 2]. Values which are not specified were interpolated with *MATLAB*.

3.2.1 Forced convection

Here we determine the influence of the fluid temperature and also the velocity of the fluid.

For the following calculations we assume a horizontal flow against a plane sheet with a blunt edge. For this assumption we can use formula 3.4 if the Reynolds number is smaller than 10^7 [13, page Gd 1]. So we have to look at the Reynolds number that can be calculated with formula 3.5. To evaluate the largest Reynolds number Re_{max}, we choose the maximum values for the numerator and the minimal value for the denominator. In a temperature range from -30 °C to +15 °C (operating range of the humidity and temperature sensor), a fluid velocity (w_∞) range from 0 to 45 $\frac{m}{s}$ and a maximum geometric length L_{max} of 0.15 m. Those values are $w_{\infty,max} = 45 \ \frac{m}{s}$, $x_{max} = 0.15$ m and $\nu_{min,air} = 109.4 \cdot 10^{-7} \ \frac{m^2}{s}$.

$$Nu \ = \ \frac{0.037 \cdot Re^{-0.2} \cdot Re \cdot Pr}{1 \ + \ 12.7 \cdot \sqrt{0.037 \cdot Re^{-0.2}} \cdot (Pr^{2/3} \ - \ 1)} \tag{3.4}$$

$$Re \ = \ \frac{w_\infty \cdot L}{\nu} \tag{3.5}$$

$$Re_{max,air} \ = \ \frac{w_{\infty,max} \cdot L_{max}}{\nu_{min,air}} \ = \ \frac{45 \ \frac{m}{s} \cdot 0.15 \ m}{109.4 \cdot 10^{-7} \ \frac{m^2}{s}} \ = \ 6.170018 \cdot 10^5$$

The value for Re_{max} is below 10^7, therefore we can use formula 3.4. The last missing quantity is the heat transfer coefficient α. This one can be calculated with formula 3.6, with L as the characteristic length of the sheet in flow direction. Because our sheet is a circle and the power for a turbulent flow is indirect proportional to the length, we choose $L = d/2 = 0.075$ m for the following calculations.

$$\alpha \ = \ \frac{Nu \cdot \lambda}{L} \tag{3.6}$$

Finally we get our needed power to keep the heating unit at a certain temperature if the surrounding fluid is dry air.

$$P_{air,forced}(w_\infty, T_{air}) \ = \ \alpha_{air}(w_\infty, T_{air}) \cdot A_{Heater} \cdot [T_{Heater} \ - \ T_{air}]$$

Figure 3.2 depicts the calculation result from $MATLAB$, for a selected surface temperature of +4 °C. For example two values from the graph are

$$P_{\text{air,forced}}\left(45\ \frac{\text{m}}{\text{s}},\ -30\ \text{°C}\right)\ =\ 120.6\ \text{W},$$

$$P_{\text{air,forced}}\left(0.0001\ \frac{\text{m}}{\text{s}},\ -30\ \text{°C}\right)\ =\ 6.291\ \text{mW}.$$
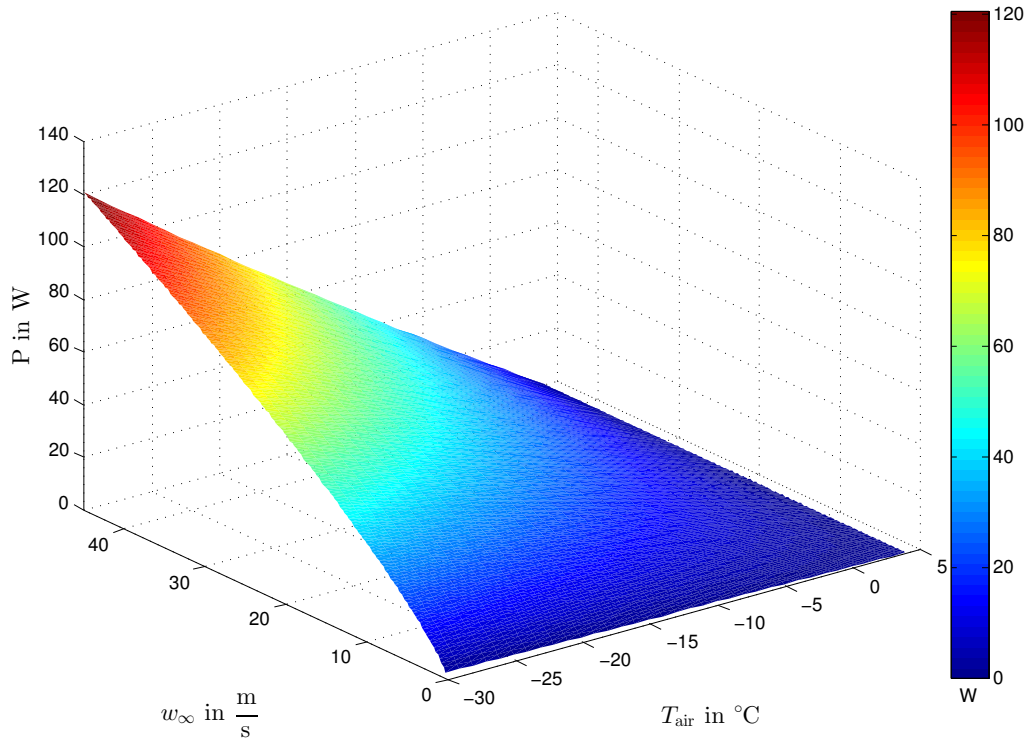

Figure 3.2: Power to keep the surface temperature at 4 °C, for dry air as fluid.

From the graph we can observe that the maximum electrical power, which is necessary to keep the surface of the heating unit at 4 °C is 120.6 W. Unfortunately the segment resistance of the realized heating unit $R_{\text{segment,real}}$ has about 34 Ω at room temperature and is lager than the analytical one on page 10. Thus for a resistance of about 31 Ω at zero degree Celsius for $R_{\text{segment,real}}$ a maximum voltage of almost 22 V is needed instead of 17 V.

$$V\ =\ \sqrt{P\cdot R_{\text{real}}}\ =\ \sqrt{\frac{P}{8}\cdot R_{\text{segment,real}}}\ =\ \sqrt{\frac{120.6\text{W}}{8}\cdot 31\ \Omega}\ =\ 21.6177\ \text{V}$$

3.2.2 Free convection

As can be seen from the value at page 13, for a very small velocity there is almost no power needed. In this section we determine the influence just for the fluid temperature. For a horizontal plane sheet which heats the bottom side the formulas 3.7 to 3.13 can be used [13, page Fa 1 - Fa 4]. Ra and Gr are the Rayleigh respectively the Grashof number and both are unit-less. The values Pr_{m}, ν_{m} and λ_{m} for the mean temperature can be calculated with formula 3.10

$$Nu_{\mathrm{free}} \;=\; 0.6 \cdot [Ra \cdot f_1(Pr_{\mathrm{m}})]^{\frac{1}{5}} \tag{3.7}$$

$$f_1(Pr_{\mathrm{m}}) \;=\; \left[1 \;+\; \left(\frac{0.492}{Pr_{\mathrm{m}}} \right)^{\frac{9}{16}} \right]^{-\frac{16}{9}} \tag{3.8}$$

$$Ra \;=\; Pr_{\mathrm{m}} \cdot Gr \tag{3.9}$$

$$X\,(T_{\mathrm{m}}) \;=\; \frac{X\,(T_{\mathrm{Heater}}) \;+\; X\,(T_{\mathrm{Fluid}})}{2} \tag{3.10}$$

The Grashof number can be calculated with the temperature difference ΔT and the volumetric thermal expansion coefficient β, which are also taken from [13, page Dbb 2].

$$Gr \;=\; \frac{g \cdot L_{\mathrm{free}}^3}{\nu_{\mathrm{m}}^2} \cdot \beta \cdot \mid \Delta T \mid \tag{3.11}$$

For the free convection the length L has to be replaced by the ratio between area A and perimeter P and can be calculated by equation 3.12.

$$L_{\mathrm{free}} \;=\; \frac{A_{\mathrm{Heater}}}{P_{\mathrm{Heater}}} \;=\; \frac{r_{\mathrm{Heater}}^2 \cdot \pi - 4 \cdot r_{\mathrm{ventilation}}^2 \cdot \pi}{2 \cdot \pi \cdot r_{\mathrm{Heater}} + 8 \cdot \pi \cdot r_{\mathrm{ventilation}}} \tag{3.12}$$

$$P_{\mathrm{free}} \;=\; \frac{Nu_{\mathrm{free}} \cdot \lambda_{\mathrm{m}}}{L_{\mathrm{free}}} \cdot A_{\mathrm{Heater}} \cdot (T_{\mathrm{Heater}} - T_{\mathrm{Fluid}}) \tag{3.13}$$

Formula 3.7 can be used in a range of $10^3 < Ra \cdot f_1(Pr_{\mathrm{m}}) < 10^{10}$. For our calculations the minimum value is $8.29 \cdot 10^3$ and the maximum one is $22.53 \cdot 10^3$. The calculation result for free convection is depicted in figure 3.3.

To keep the heating unit at +4 °C, for a air temperature of -30 °C, a power of 2.71 W is needed. Compared with the value from page 13, for almost still air, the power for free convection is 430 times higher.
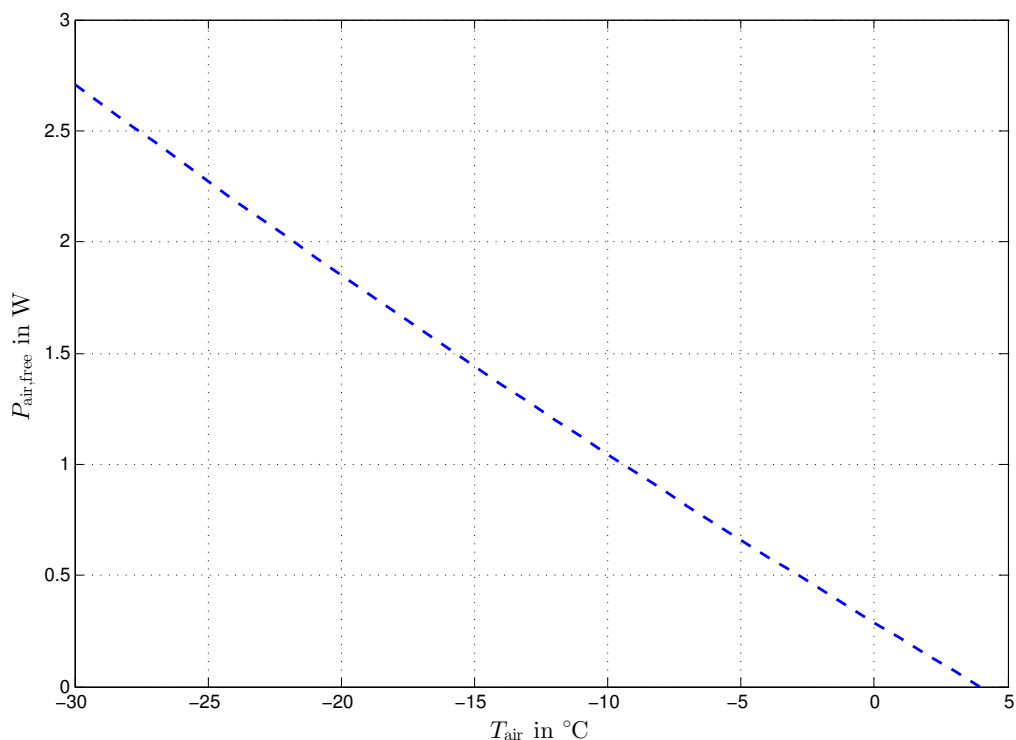

Figure 3.3: Power to keep the surface temperature at 4°C for free convection

For both, the free and forced convection, the influence of snow and wet air as a function of temperature was observed. These two aspects are not discussed further, since their influence are very small. For example in one cubic meter air at 0 °C there is just 4.868 g water and the water content decreases with the temperature. For dense snowfall it is almost the same. There are approximately 7 g snow in one cubic meter air.

3.2.3 Influence of an ice layer

The operating range of the humidity and temperature sensor is -30 ℃ to +70 ℃. Therefore the heating unit is dimensioned for a minimum temperature of -30 ℃. In this subsection a simplified calculation for the needed time which is necessary to get rid of an ice layer is discussed. This calculation neglects any kind of convection. The values for the necessary quantities and also the calculation are taken from [14, page 47], with ρ_{ice} as the density of ice at -30 ℃, c_{ice} the specific heat capacity, $r_{S,ice}$ the specific melting heat and d_{ice} the thickness of the ice layer.

To get the ice at the melting temperature the thermal energy Q_1 is needed.

$$Q_1 \; = \; \rho_{ice} \cdot c_{ice} \cdot A_{Heater} \cdot d_{ice} \cdot (T_{Heater} \; - \; T_{Ambient}) \qquad (3.14)$$

$$Q_1(d_{ice}) \; = \; 921.5 \, \frac{kg}{m^3} \cdot 1.93 \, \frac{kJ}{kg \cdot K} \cdot 0.01594 \, m^2 \cdot d_{ice} \cdot (0 \, ℃ - (-30 \, ℃))$$

$$Q_1(d_{ice}) \; = \; 850.29 \, \frac{kJ}{m} \cdot d_{ice}$$

The thermal energy Q_2 is needed to melt the ice.

$$Q_2 \; = \; \rho_{ice} \cdot r_{S,ice} \cdot A_{Heater} \cdot d_{ice} \qquad (3.15)$$

$$Q_2(d_{ice}) \; = \; 921.5 \, \frac{kg}{m^3} \cdot 333.4 \, \frac{kJ}{kg} \cdot 0.01594 \, m^2 \cdot d_{ice} \; = \; 4896.145 \, \frac{kJ}{m} \cdot d_{ice}$$

The whole thermal energy Q_{melt} is

$$Q_{melt}(d_{ice}) \; = \; Q_1(d_{ice}) \; + \; Q_2(d_{ice}) \; = \; 5746.435 \, \frac{kJ}{m} \cdot d_{ice} \qquad (3.16)$$

$$P_{max} \cdot t_{melt} = Q_{melt}(d_{ice}) \qquad \Rightarrow \qquad t_{melt}(d_{ice}) = \frac{Q_{melt}(d_{ice})}{P_{max}} \qquad (3.17)$$

In figure 3.4 the needed time to melt the ice layer as a function of its thickness is depicted. The calculation is made with a power supply that fulfills the criteria for the forced convection. Thus a power supply with 24 V and a maximal thermal power P_{max} of 239.187 W is chosen. It should be mentioned that our heating unit heats the bottom side. Thus if the melting process starts, the gravity accelerate the elimination of the ice by dropping down.
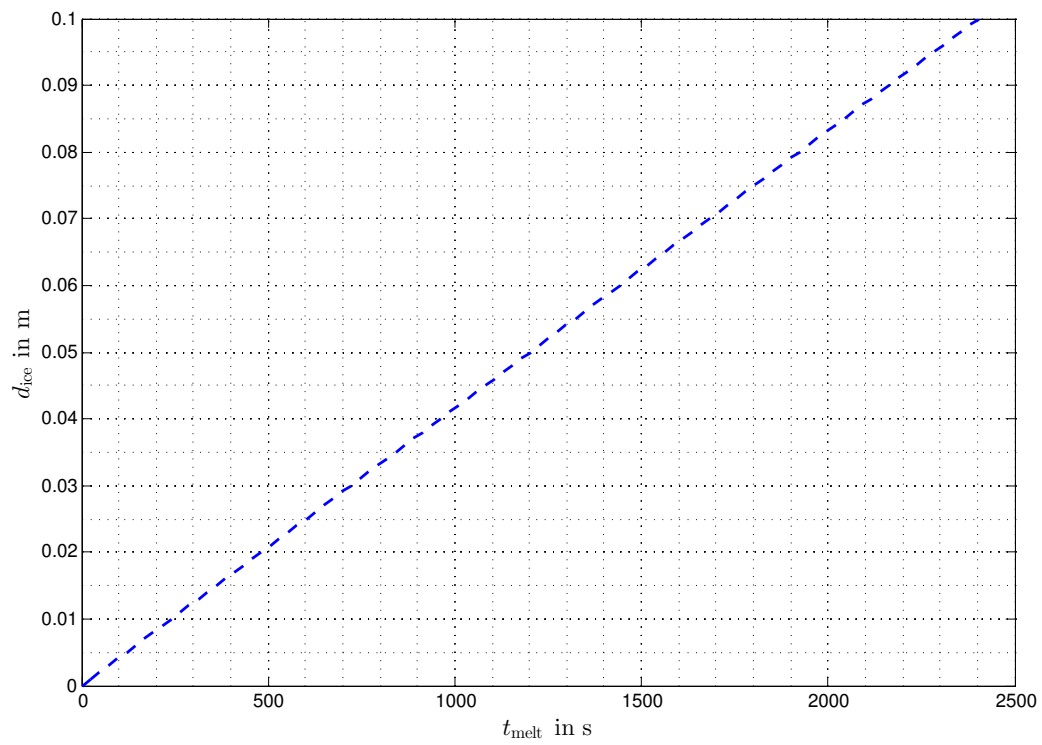
16

Figure 3.4: Simplified result for the needed time to melt an ice layer as a function of its thickness.

3.3 CFD - Model verification

To verify the calculations from section 3.2.1 the program *COMSOL* version 4.3a is used. The area of the heating unit in the previous calculations is fitted to those of the simulation. For an area A of 0.075 m², a fluid velocity w_∞ of 45 $\frac{m}{s}$ and a fluid temperature of -30 °C a power of 567.4 W is needed to keep the surface temperature at +4 °C. In figure 3.5 the result for a plate with a length of 0.075 m and a depth of 1 m is depicted. The inlet for the turbulent flow is on the left side. So as expected the edge on the left (x = 0.025 m) is the coldest point of the plate and the edge facing away from the wind is the hottest point. Figure 3.6 shows an enlargement approximately 1 cm right from the wind faced edge. From this distance the surface temperature is above +4 °C. Thus we can say the calculations fits with the simulation.

The *Non-Isothermal turbulent flow* - physic is used. Because the heat transfer at the surface is of interest the *Low Reynolds k-ε* model is selected, which does not use wall functions. To get correct results the *dimensionless distance to cell center* (figure 3.7), whose value is generated by default, should be less than 0.5 everywhere [15]. For the plate the *Thermal Insulation* boundary condition is chosen.
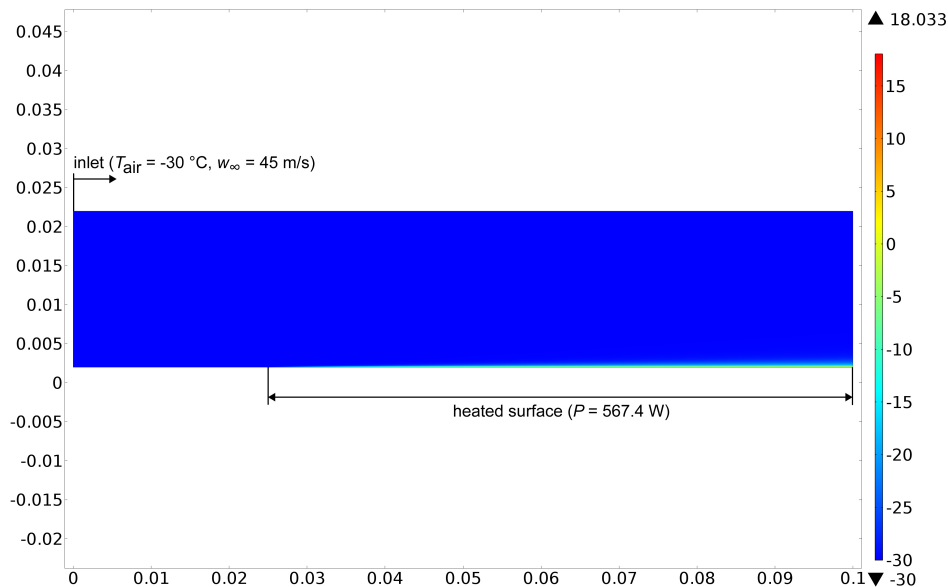

Figure 3.5: Surface temperature of a turbulent overflowed heated plate in degree Celsius.
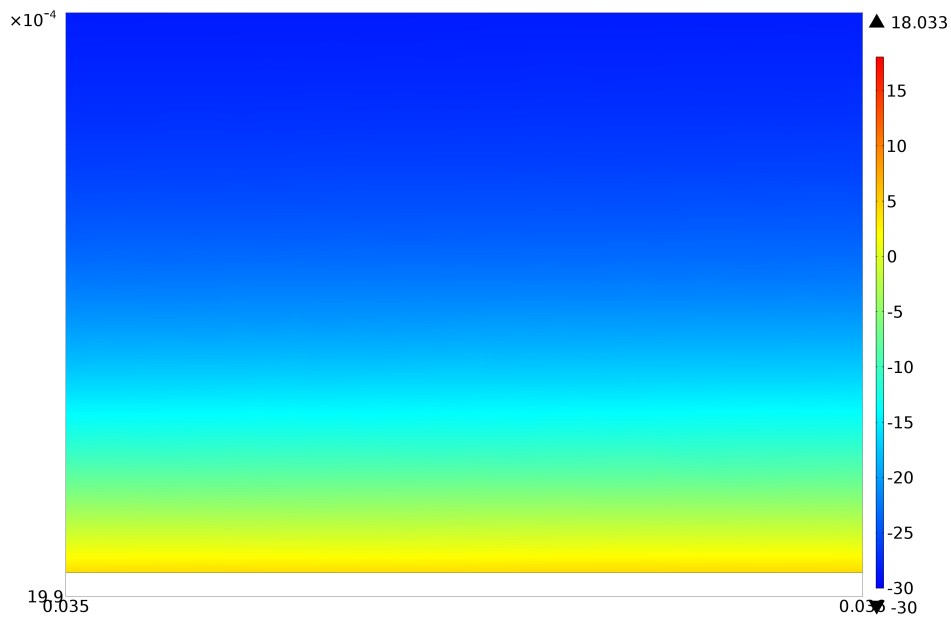
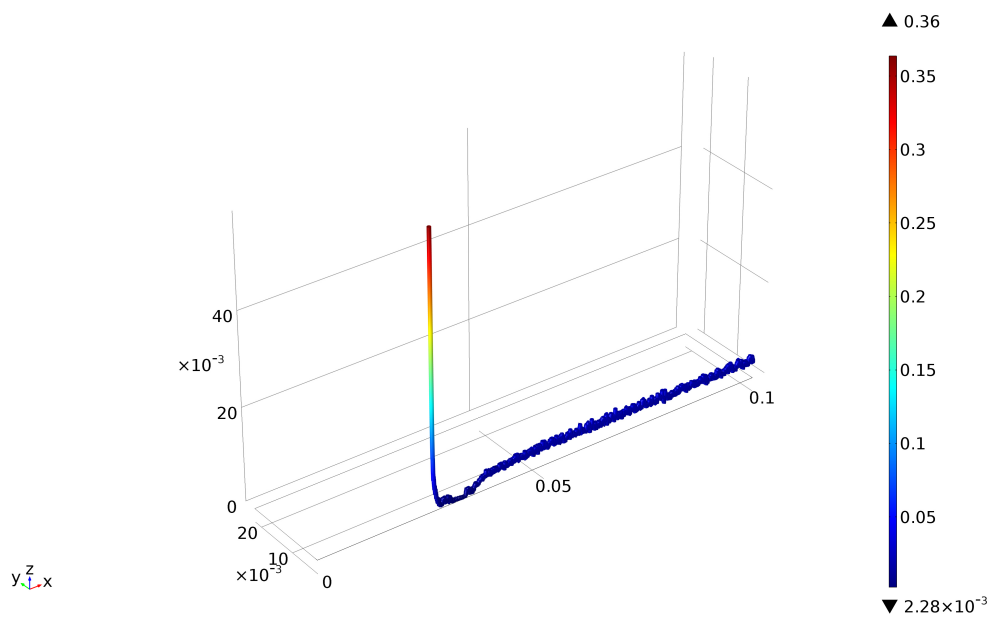Figure 3.6: Surface temperature 1 cm right from the wind faced edge in degree Celsius.

Figure 3.7: Dimensionless distance to cell center with the highest value at the wind faced edge.

3.4 CFD - Housing - simulations

To observe the fluid behavior and also the heat transfer in the solid parts (acrylic glass) of the housing, the physic *Conjugate Heat Transfer* and the *Low Reynolds* k-ε model are used. Because the used *COMSOL* version 4.3a does not support an interior fan for a turbulent flow, the problem is split up into two separate problems.

3.4.1 Problem 1: Outside

For a further investigation of the needed power a *Boundary Heat Source* is defined at the bottom edge of a 75 mm long acrylic glass with a hight of 20 mm. In figure 3.8 the temperature across the heated acrylic plate on the right side can be seen. To the left of it a non heated acrylic plate with the same length is placed. The structure is overflowed by a turbulent stream with 45 $\frac{m}{s}$ and -30 °C from the left side. A power of 1000 W is needed to get the same temperature gradient across the surface as in section 3.3. That is about two times more than evaluated by the analytical calculations. So for a power supply of 24 V the device cannot be used in the whole temperature and velocity range. The additional power is needed to heat the acrylic glass.
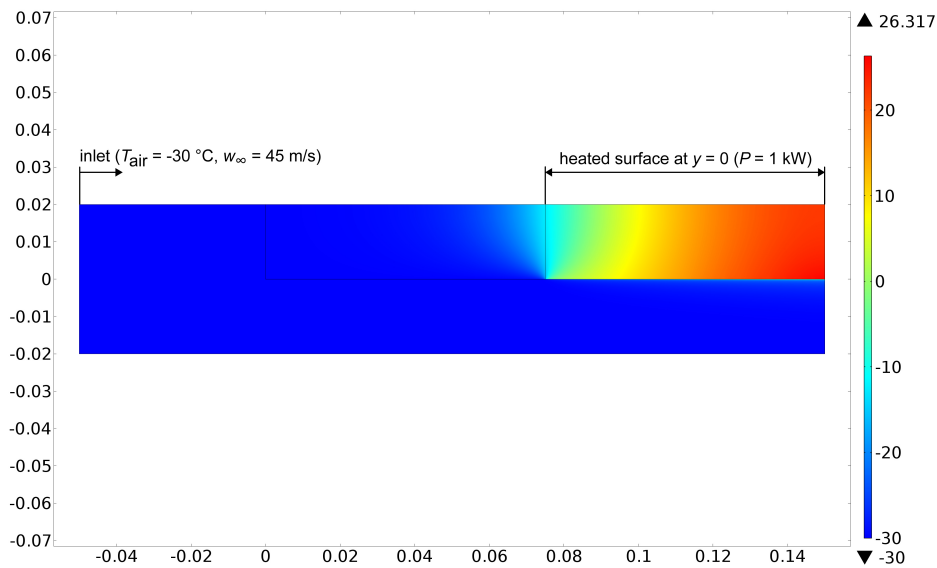

Figure 3.8: Temperature in degrees Celsius for a bottom heated acrylic glass.

In figure 3.9 the bottom side of the housing including two ventilation holes can be seen. It has a total length of 150 mm (diameter of the „real" heating unit) and two ventilation holes with 23.5 mm. Each solid acrylic glass element has a length of 25.75 mm and a high of 20 mm. Just the two elements which are facing away from the wind are heated. The inlet is on the left side and has a velocity w_∞ of 15 $\frac{m}{s}$ and a temperature of -30 °C. In this simulation for the heated elements a constant temperature is used. It should be mentioned that the gap in the plate results in a higher need of power to keep the surface temperature at +4 °C. This is neglected for further considerations because the ventilation holes lower the whole surface just by a tenth.

The fluid flow is depicted in figure 3.10. For the fans the boundary condition *Outlet* is chosen. The left fan blows the fluid upwards and the right one downwards which are represented by the gap top center respectively top right. Both with a velocity (w_{in} and w_{out}) of 0.884 $\frac{m}{s}$.

The *dimensionless distance to cell center* in figure 3.11, is for the whole region smaller than 0.5.
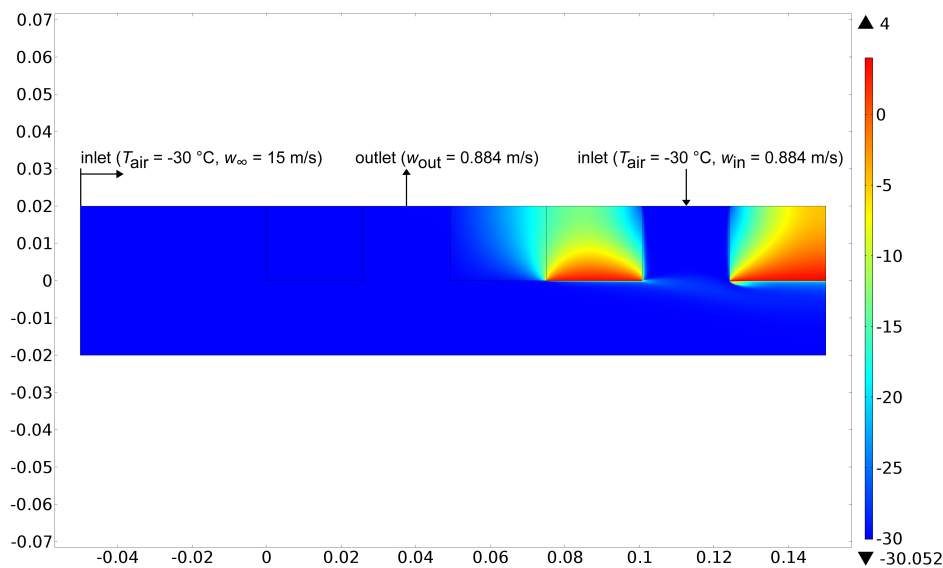

Figure 3.9: Temperature gradient in the bottom of the housing in degree Celsius with active ventilation (w_{in}, w_{out}). Constant temperature of 4 °C at $y = 0$, from $x = 0.075$ to 0.10075 m and from $x = 0.12425$ to 0.15 m.
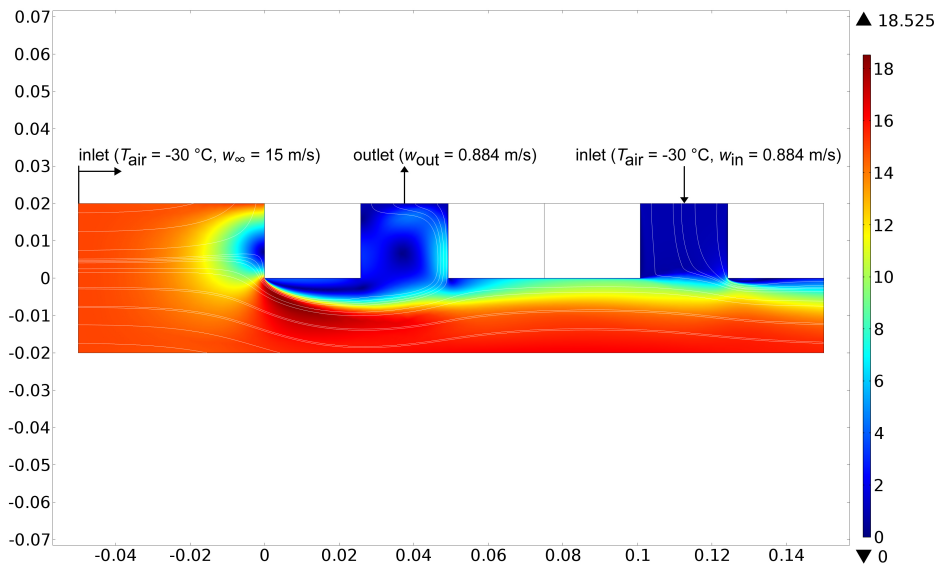
Figure 3.10: Velocity in $\frac{m}{s}$ with active ventilation (w_{in}, w_{out}). Thus the white streamlines leaving the fluid into the „housing" top center and reentering top right.
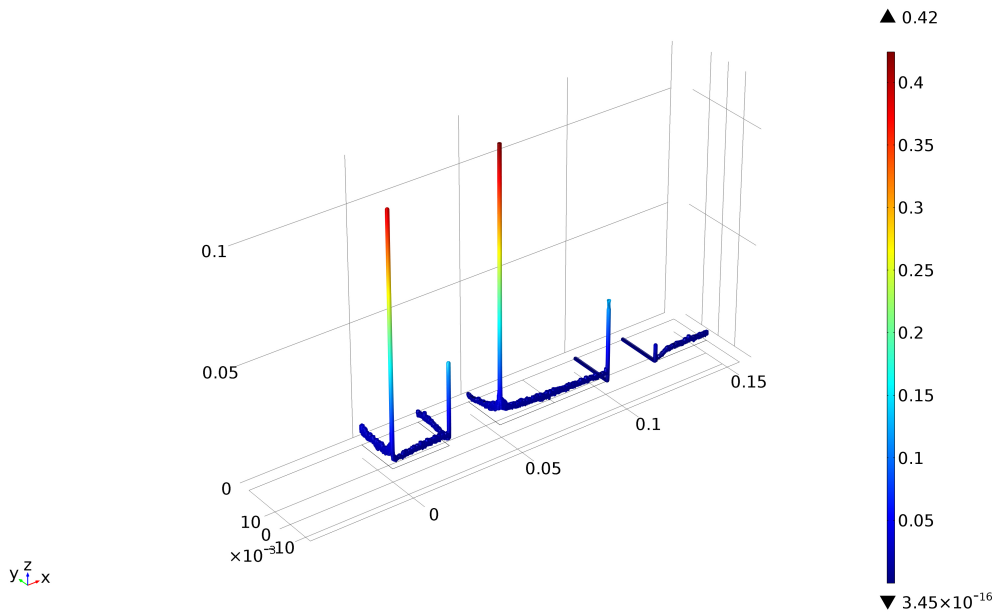

Figure 3.11: Dimensionless distance to cell center with the second highest value for the wind faced edge and the highest for the left side of the housing inlet.

3.4.2 Problem 2: Inside

Figures 3.12 to 3.15 are showing the results inside the housing. Just the inlet on the left side has both velocity components. A horizontal component $w_{in,x}$ with approximately 2.5 $\frac{m}{s}$ and a vertical one $w_{in,y}$ with 0.884 $\frac{m}{s}$. The value for the horizontal velocity of the inlet is determined from figure 3.10.

Just the fan facing away from the wind is turned on because the measurement results should not be influenced by the warming of the fluid, caused by the movement of the fan. Unfortunately the simulation attempts with just an horizontal velocity component for the inlet and both components for the outlet cancel with an error. Why the horizontal component is important can be seen in figure 3.15. The meteorologic sensor take place in the middle of the housing and is mounted on the top. Therefore a frustum is used to direct the fluid flow over the sensor. This is illustrated in figure 3.13.
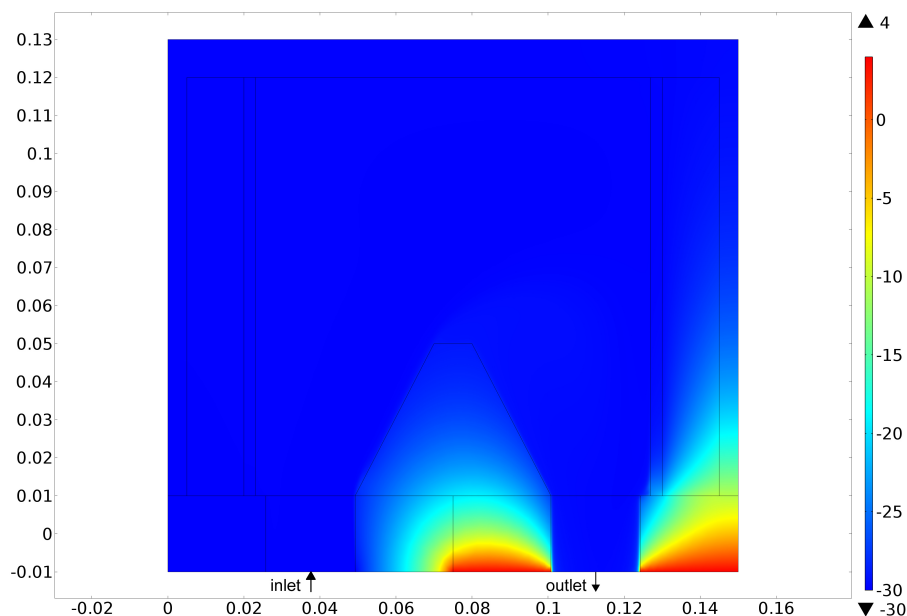
Figure 3.12: Temperature gradient inside the housing and the solid parts in degrees Celsius. Inlet: $w_{in,x} = 2.5$ $\frac{m}{s}$, $w_{in,y} = 0.884$ $\frac{m}{s}$, $T_{air} = -30$ °C. Outlet: $w_{out,y} = 0.884$ $\frac{m}{s}$. Constant temperature of 4 °C at $y = -0.01$, from $x = 0.075$ to 0.10075 m and from $x = 0.12425$ to 0.15 m.
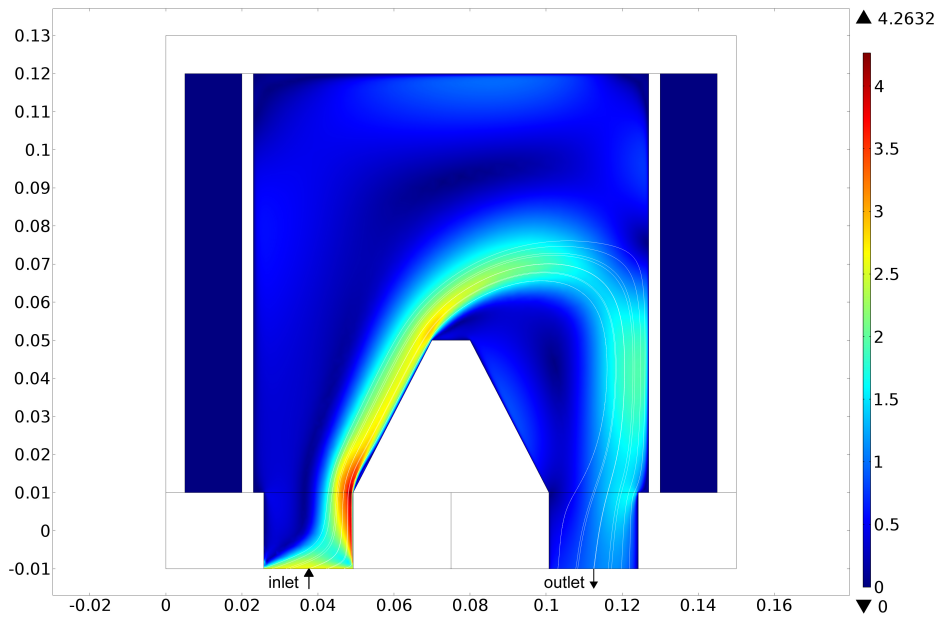
Figure 3.13: Velocity in $\frac{m}{s}$ and forced fluid velocity field (white streamlines) over a frustum. Inlet: $w_{in,x} = 2.5 \frac{m}{s}$, $w_{in,y} = 0.884 \frac{m}{s}$, $T_{air} = $ -30 °C. Outlet: $w_{out,y} = 0.884 \frac{m}{s}$.

Figure 3.14: Dimensionless distance to cell center
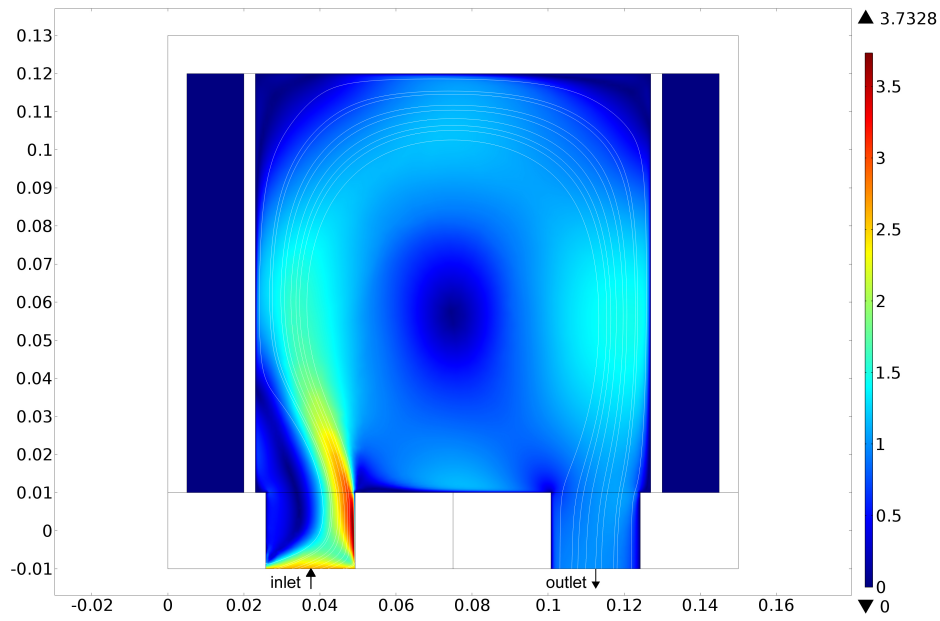
Figure 3.15: Velocity field in $\frac{m}{s}$ and velocity field (white streamlines) without a frustum. Inlet: $w_{\text{in,x}} = 2.5$ $\frac{m}{s}$, $w_{\text{in,y}} = 0.884$ $\frac{m}{s}$, T_{air} = -30 °C. Outlet: $w_{\text{out,y}} = 0.884$ $\frac{m}{s}$.

3.5 Heating circuit

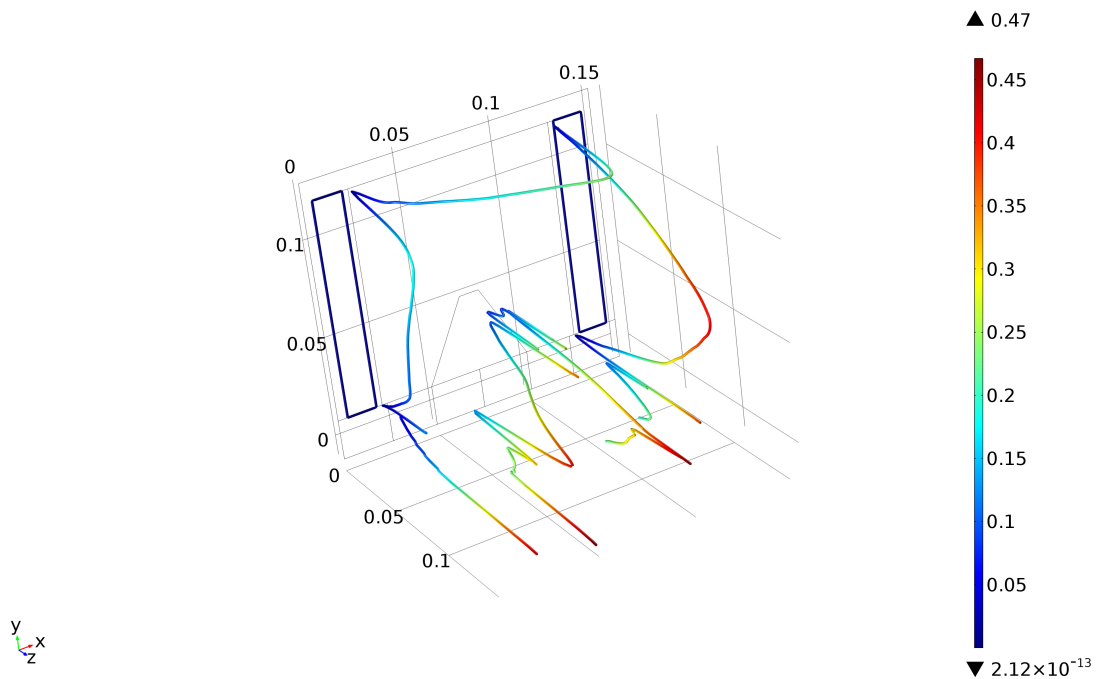A simplified schematic how the heating circuit is realized is depicted in figure 3.16. The relay S_{DPDT} is responsible for changing between the capacitive measurement, with the contacts EXC and C_{IN}, and the heating process. The relay positions in figure 3.16 show the heating process setting. With the relay S_{SPST} the outer ends of one segment (figure 3.1) can be closed for the heating process, or opened for the measurement of the capacitance. Each of the two resistors $R_{\mathrm{H}}/2$ represents one half of the whole heating resistor. The both relays are controlled by a low side switch (LSS) which is represented by M_3. For each segment one S_{DPDT}, one S_{SPST} and one low side switch M_3 is needed.

The heating process is implemented with the two MOSFETs M_1 and M_2. The n - channel MOSFET M_2 is accessed by a Pulse Width Modulation PWM. Thus the voltage curve across the resistors $R_{\mathrm{H}}/2$ is modulated by PWM and can be adjusted according to the environmental conditions.
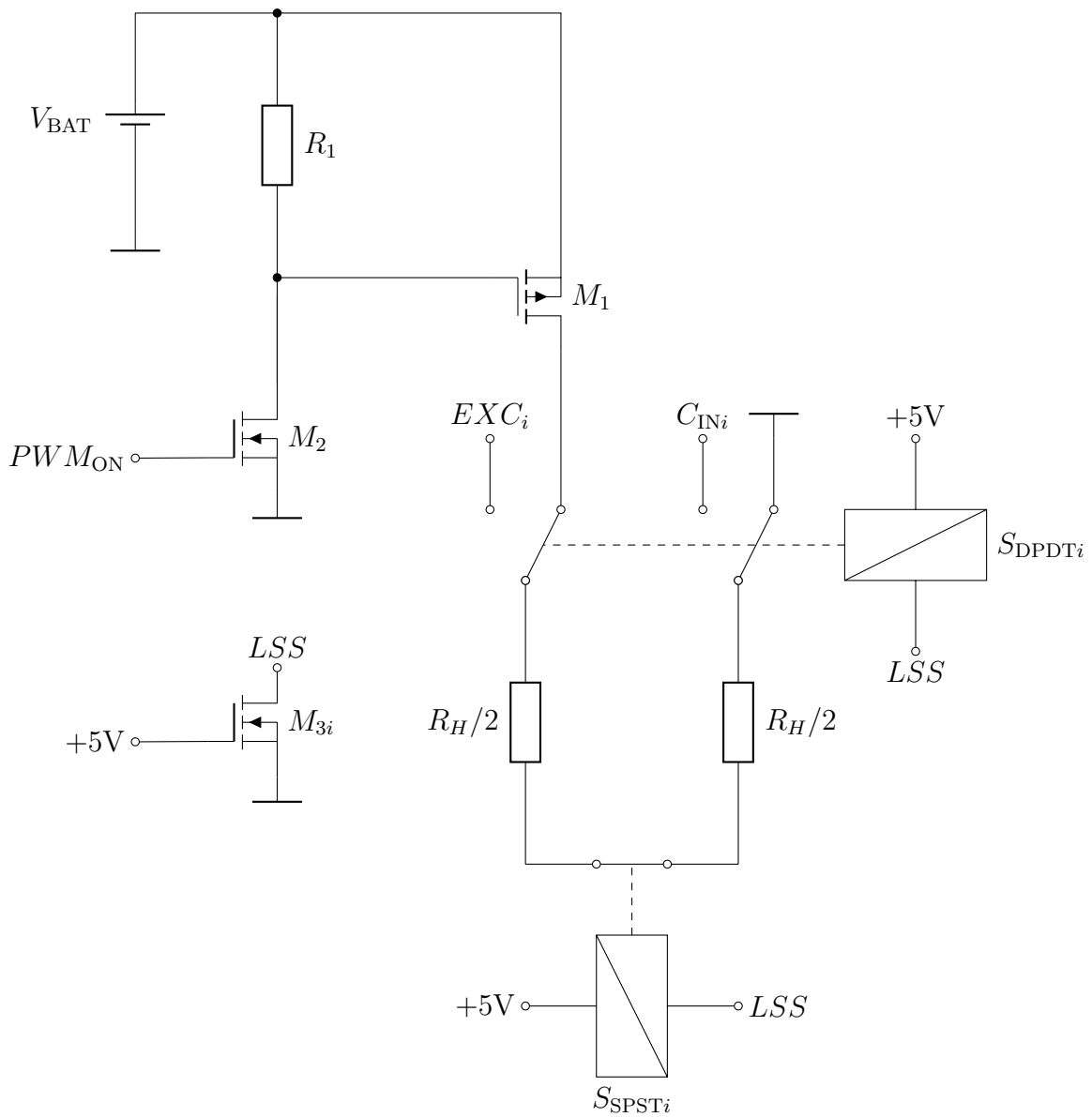
Figure 3.16: Simplified schematic of the realized circuit for the capacitance measurement and heating process.

3.6 De-icing

To investigate if the heating unit is capable of getting rid of an ice layer which covers the whole surface, experiments in a climate cabinet are made. In table 3.2 two successful melting processes are listed. Figure 3.17 shows the ice covered device at -10 °C right before the heating process starts and 3.18 seven minutes and fifty-one seconds later. During the de-icing process all segments are heated and the process is executed till the the connection between the heating unit and ice layer is loosened and the ice drops down.

Temperature	t_{melt} in min	P_{melt} in W
-10 °C	7:51	~ 64
-15 °C	11:14	~ 65

Table 3.2: Values for two successful de-icing attempts

The tests show that there should not exist connections between the ice layer and non heated parts. Otherwise it is not possible to get rid of the whole ice. Figure 3.19 shows the heating unit at -20 °C after 40 minutes heating. By having a look at the ventilation holes, which are covered with blue tape, a connection between the ice and the non heated tape can be seen.
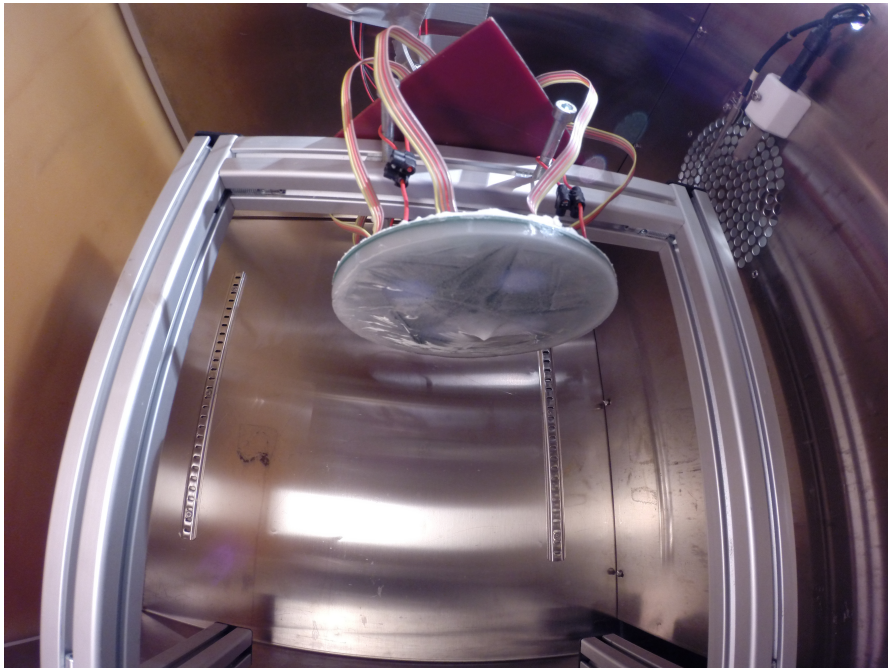
Figure 3.17: Ice covered heating unit at -10 °C with the CONTROL - PCB on top of the aluminum profile.
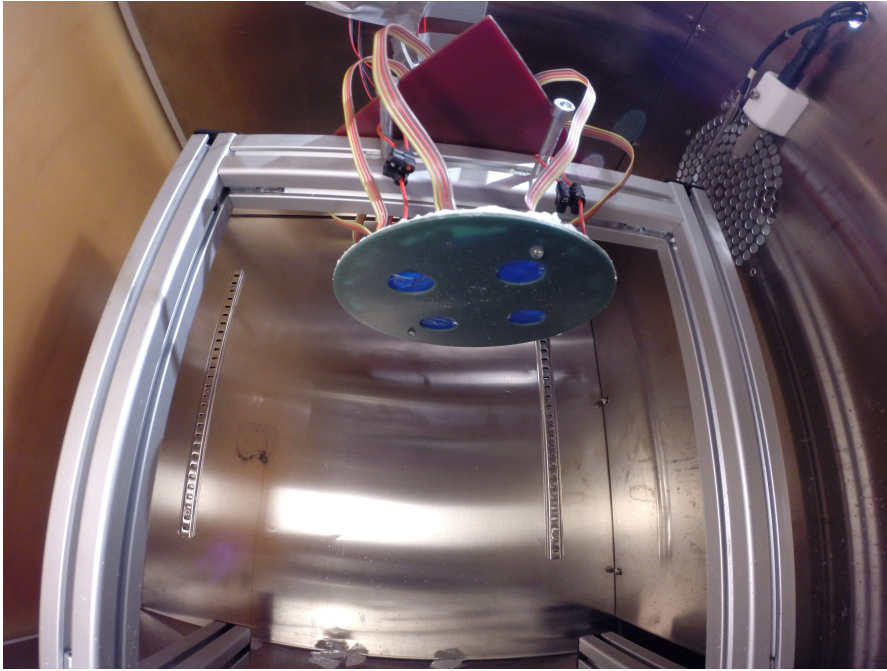
Figure 3.18: Heating unit after 7 minutes and 51 seconds heating at -10 ℃.
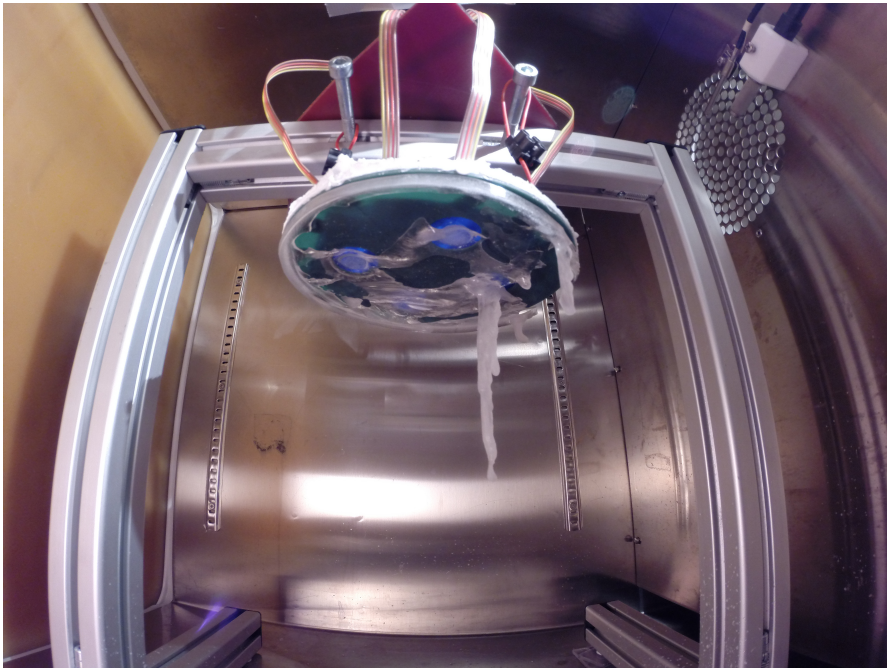
Figure 3.19: Failed de-icing attempt after 40 minutes heating, with approximately 60 W at -20 ℃.

The VIAs of the heating unit are not covered with solder resist. The combination of melting water and direct current, which is supplied to heat the surface, causes electrolysis. This damage of the VIAs can be seen in figure 3.20 and causes a malfunction of two segments.

A failed de-icing process caused by the malfunction of the two segments can be seen in figure 3.21. There are still connections between the non heated segments and the ice. The non heated segments are adjacent to the two segments in the lower left corner. The copper traces are the boundary of the segments.
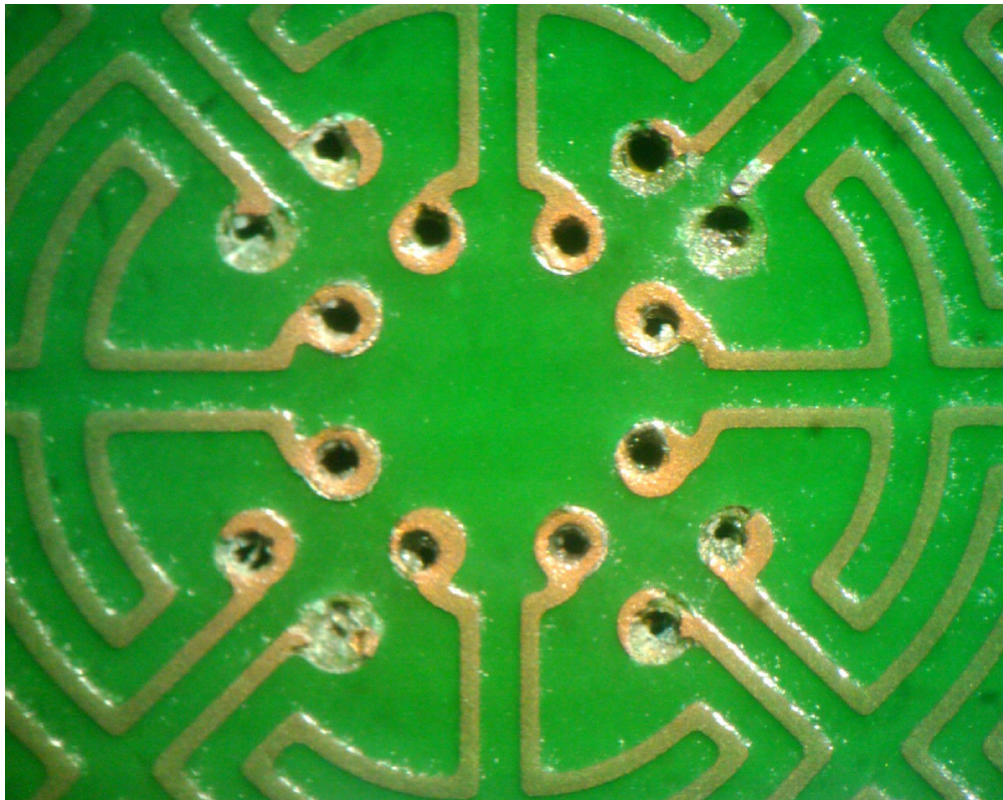
Figure 3.20: Damaged VIAs in the middle of the heating unit caused by electrolysis.
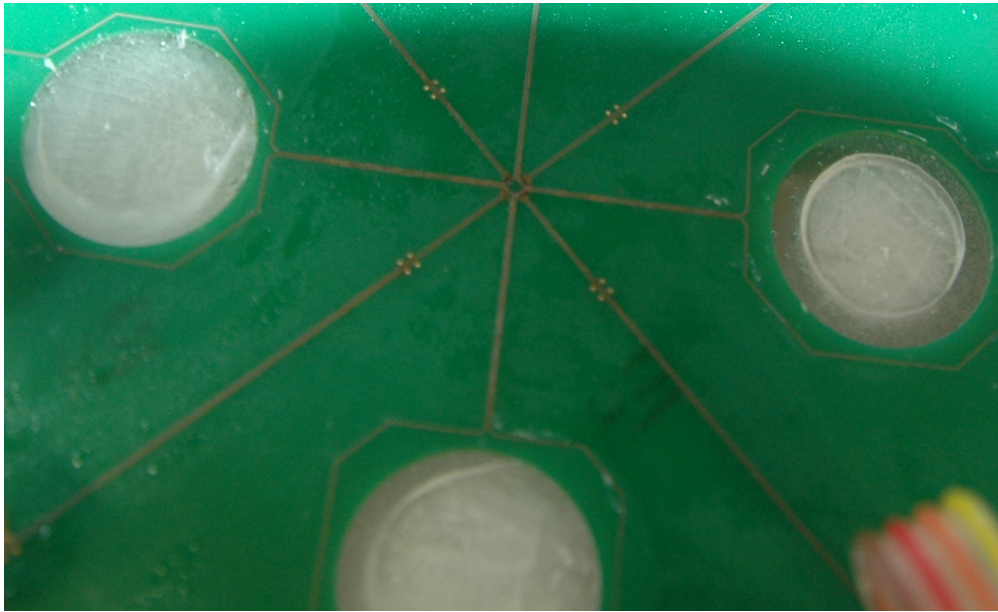
Figure 3.21: Failed de-icing attempt caused by the malfunction of two segments. There are two connections between PCB and ice left.

3.7 Distortion of the meteorological temperature

The main task of the whole work is to determine reliable meteorological values. Thus the temperature change caused by the heating process is of interest. Therefore the whole weather and radiation shield (figure 3.22) is placed in the climate cabinet. It consists of the HEATING - PCB at the bottom side of the acrylic glass cylinder, a second (STACK) PCB on top of it, including a digital temperature sensor, and the connectors for the four fans inside the housing. Attached to a separate cylinder the meteorological temperature sensor is placed in the middle of the lower half. The heating unit is connected to the CONTROL - PCB in the top half of the housing.
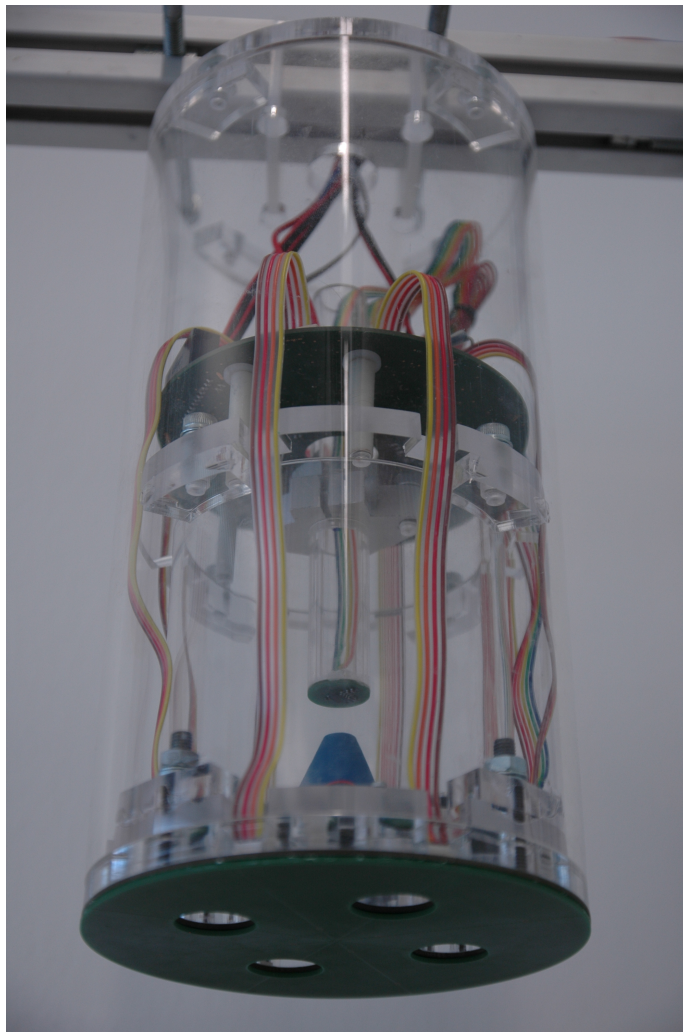
Figure 3.22: Complete weather and radiation shield with the heating unit at the bottom.

Figure 3.23 to 3.25 show the temperature behavior before, during and after the heating process. For the following test just one half of the heating unit is powered with approximately 11.5 W. During the whole measurement the two fans related with the heated side are turned on and blow air out. In figure 3.23 the meteorological temperature before the heating process is started can be seen. As an indication if the surface of the heating unit is above zero degree Celsius, the cold junction temperature T_{cj} is observed. This temperature is measured at the middle of the STACK - PCB and is isolated with 3.2 mm FR4 material.
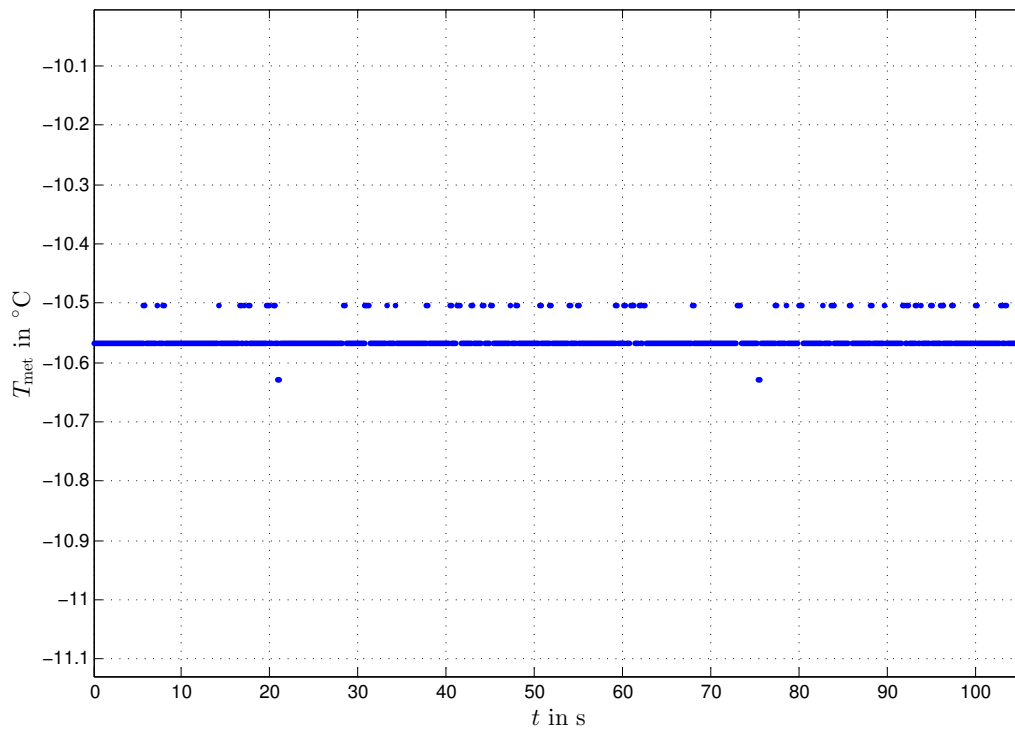
Figure 3.23: Meteorological temperature T_{met} of -10.56 °C inside the housing, before the heating process starts.

The progress of T_{cj} during the heating is depicted in figure 3.24. The progress starts with -10.63 °C and ends at 0.313 °C. The resulting meteorological temperature after the heating process is shown in figure 3.25. The temperature increases although the heating is stopped. This is caused by heating up interior the structure during the heating and not by the intake of warmth air from the hot segments. To verify this, two thermocouples are placed ∼1 cm blow the inlet respectively the outlet. By comparing the values from figure 3.23 and 3.25 it can be seen that the distortion of the meteorological temperature caused by the heating is 0.37 °C.

According to the CFD simulation on page 24 a (blue) frustum (figure 3.22) is placed in the middle of the lower half of the housing to improve the fluid stream over the meteorological temperature sensor. The depicted figures show the result with the frustum. Unfortunately there is no difference to the results without it.

It takes about 70 minutes after the heating process is stopped till the same meteorological temperature is measured again. To investigate the thermal inertia the weather and radiation shield is cooled down to -10.53 °C. Than the housing is removed from the climate cabinet and exposed to a room temperature of 23.5 °C. It takes almost three hours until the room temperature is equal to the measured temperature by the meteorological sensor.

This long duration can be explained by the thermal capacity of the acrylic glass. By using fans with a higher throughput and a suitable frustum it should be possible to shorten the needed time. The acrylic glass is just used for the prototype. By using a material with a lower thermal capacity the time should be reduced too.
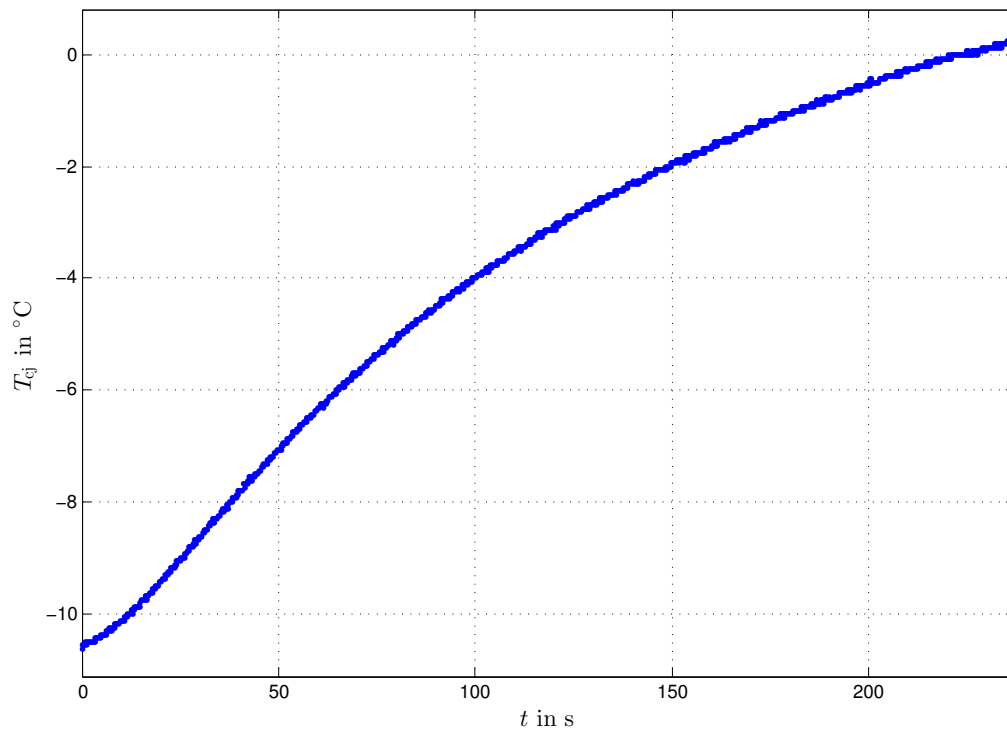
Figure 3.24: Cold junction temperature T_{cj} during the heating process. $t_{elapsed} = 237$ s, $T_{cj,min}$ = -10.63 °C, $T_{cj,max}$ = 0.313 °C.
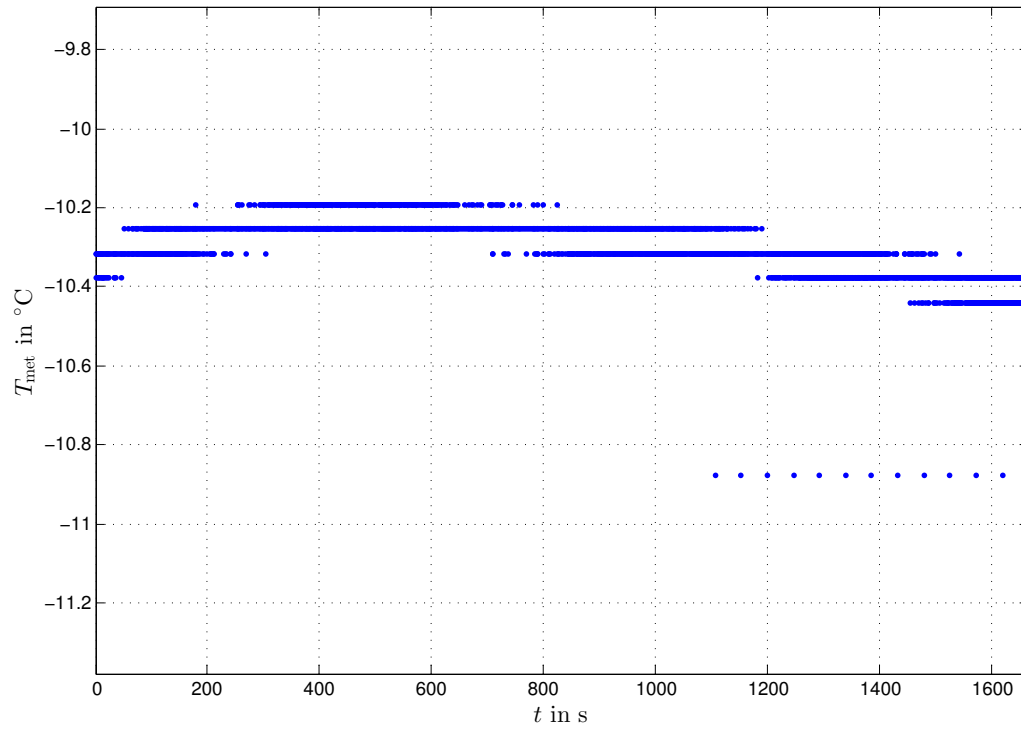
Figure 3.25: Meteorological temperature T_{met} after the heating process. $T_{met,max}$ = -10.19 ℃.

Ice detection

Lowering the power consumption of the heating unit and to avoid the formation of an ice layer demands an ice detection device. To get rid of the ice it is important to prevent non heated parts on the surface of the heating unit, as can be seen in section 3.6. To fulfill this requirement we use a capacitance measurement which uses the existing heating structure. This is the reason why the heating segments are splitted up into two parts and have a meander structure (figure 3.1). So each part can be used as an electrode for the capacitance measurement.

4.1   Electrostatic simulation

To determine the expected capacitance a *FEM* simulation is made. Therefore a 30 cm long geometry, representing the heating element, is placed in the middle of a 7 times 7.3 meter large area. The architecture of the geometry in figure 4.1 consists from bottom to top of a ground plane, 1.6 mm FR4 ($\varepsilon_r = 4.5$) and copper traces coated with solder resist ($\varepsilon_r = 3.5$). The geometry is surrounded by air and Neumann boundary conditions are used for the boarder of the area.

The capacitance is evaluated for a length l_{Comsol} of 10 cm in the middle of our geometry. This corresponds to a surface of 0.1 m^2. To determine the measurement capacitance, line integrals are placed around the copper traces with ground level in the observed section. To evaluate the driving capacitance the line integrals were placed around the copper traces with 1 V. The results are listed in table 4.1. The simulations for ice and snow are made with a layer thickness d of 5 mm. To get the expected capacitance per segment for our prototype, equation 4.1 and 4.2 are used.

$$A_{\text{Segment}} \;=\; \frac{r_{\text{Heater}}^2 \cdot \pi - 4 \cdot r_{\text{ventilation}}^2 \cdot \pi}{8} \tag{4.1}$$

$$A_{\text{Segment}} \;=\; \frac{0.075^2 \text{m}^2 \cdot \pi - 4 \cdot 0.01175^2 \text{m}^2 \cdot \pi}{8} \;=\; 0.001992 \text{ m}^2$$

$$C_{\text{Segment}} \;=\; \frac{C_{\text{Comsol}}}{l_{\text{Comsol}}} \cdot A_{\text{Segment}} \tag{4.2}$$

	Measurement Capacitance		Driving Capacitance	
Top Layer	$C_{\text{M,Comsol}}$ in $\frac{\text{nF}}{\text{m}}$	$C_{\text{M,Segment}}$ in pF	$C_{\text{D,Comsol}}$ in $\frac{\text{nF}}{\text{m}}$	$C_{\text{D,Segment}}$ in pF
Air ($\varepsilon_r = 1.00059$)	7.228	143.994	8.262	164.577
Ice ($\varepsilon_r = 3.2$)	9.079	180.864	10.076	200.730
Snow ($\varepsilon_r = 50$)	17.009	338.834	17.840	355.384
Water ($\varepsilon_r = 80$)	17.924	357.052	18.731	373.142

Table 4.1: Sensor capacitance for different top layer materials.
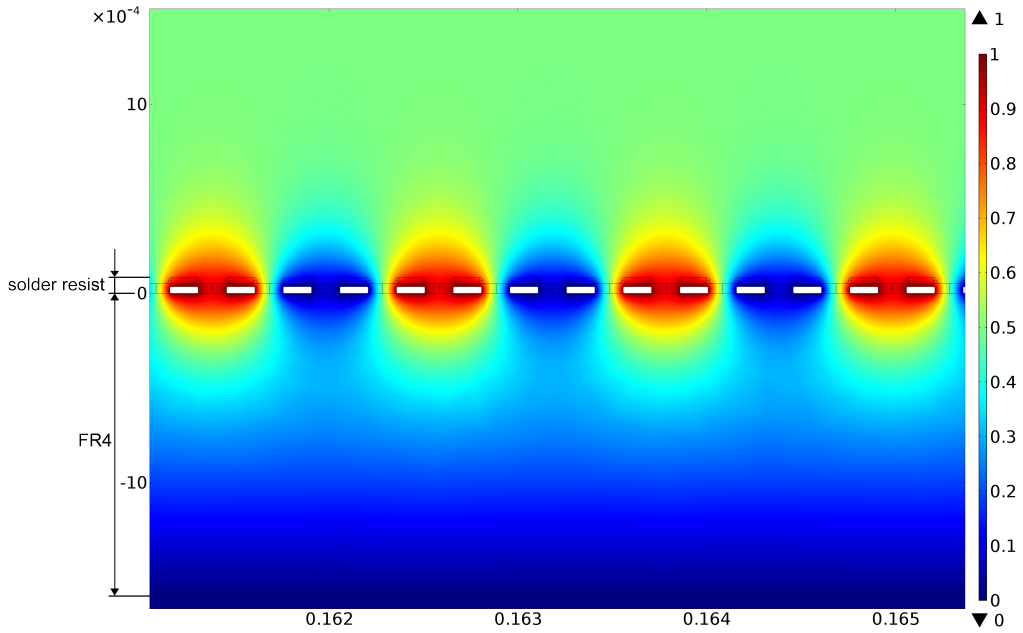
Figure 4.1: Electric potential of the ice covered sensor in V. With a ground plane at y = -16 $\cdot$ 10^{-4} m, followed by 1.6 mm FR4, solder resist covered copper traces (white holes) and a 5 mm thick ice layer on top.

4.2   Capacitance measurement circuit

In figure 4.2 the capacitance measurement circuit is displayed. By setting the gate voltage of the low side switch M_3 to zero the monostable relays S_{SPST} and S_{DPDT} change to their stable position. This corresponds with the position in figure 4.2 for the capacitance measurement. Mechanical signal relays are used instead of MOSFETs because the capacitance between open contacts is with 1 pF much smaller than the output capacitance of a MOSFET. The pins SCR and EXC are connected via a range extension circuit which is explained on page 40.
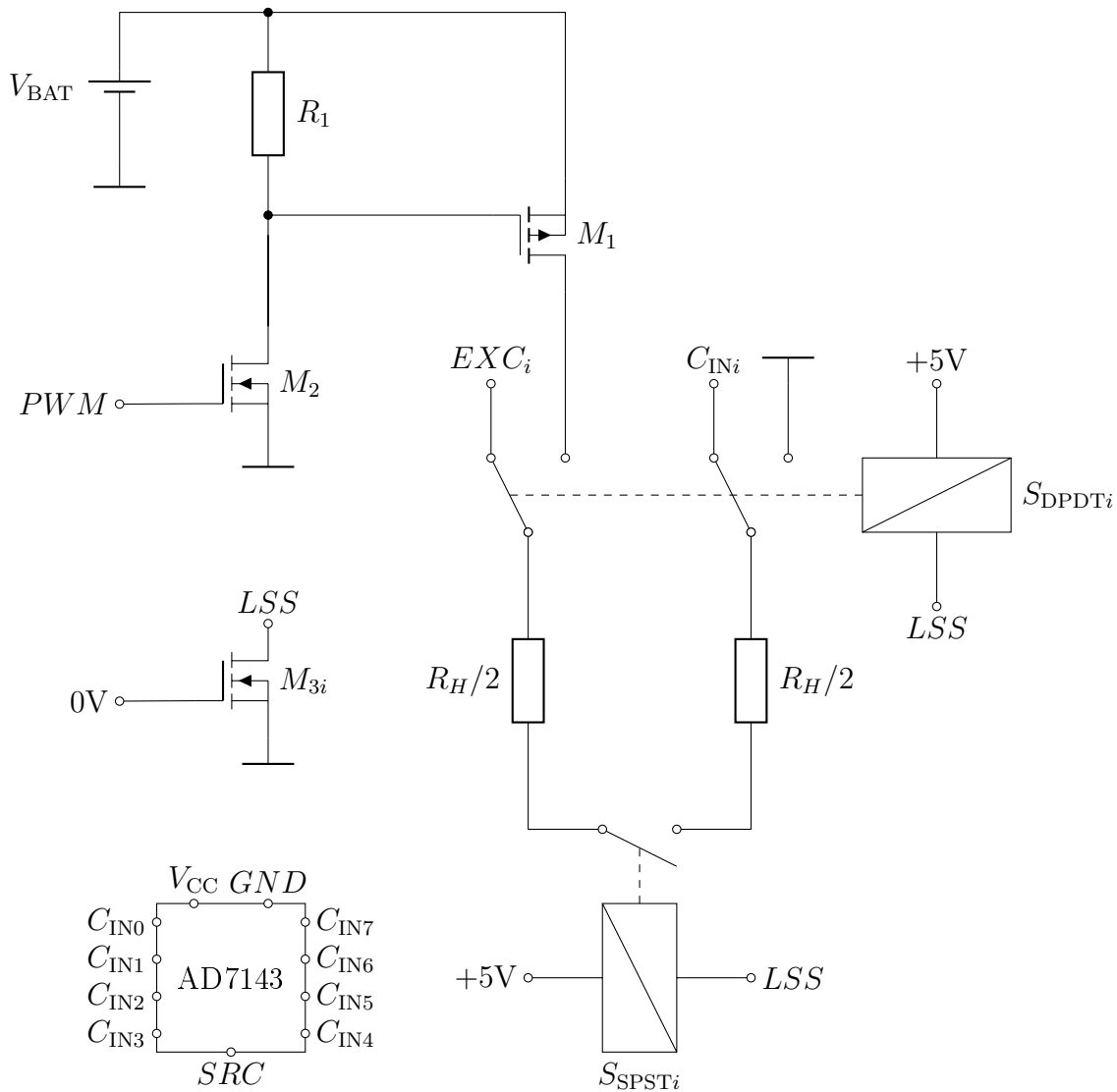
Figure 4.2: Schematic of the capacitance measurement circuit. SCR and EXC_i are connected via the capacitance range extension circuit in figure 4.3.

To measure the capacitance of the heating unit we use the AD7143, a capacitance to digital converter from *ANALOG DEVICES*. The chip has eight capacitance sensor input channels and a I²C compatible serial interface. Because the AD7143 has only an input range of ±2 pF a range extension circuit is needed. An extension circuit for an other capacitance to digital converter from *ANALOG DEVICES* is shown in [16]. A modified circuit for our model is depicted in figure 4.3. The circuit consists of an operational amplifier and a voltage divider.

The range extension circuit has to ensure that the charge transfer within the sensing capacitance C_{SENS} remains within the input range of the AD7143. To achieve this, the excitation voltage needs to be decreased by a factor of F, so that the sensing capacitance connected to the input can be increased by a factor F [16].
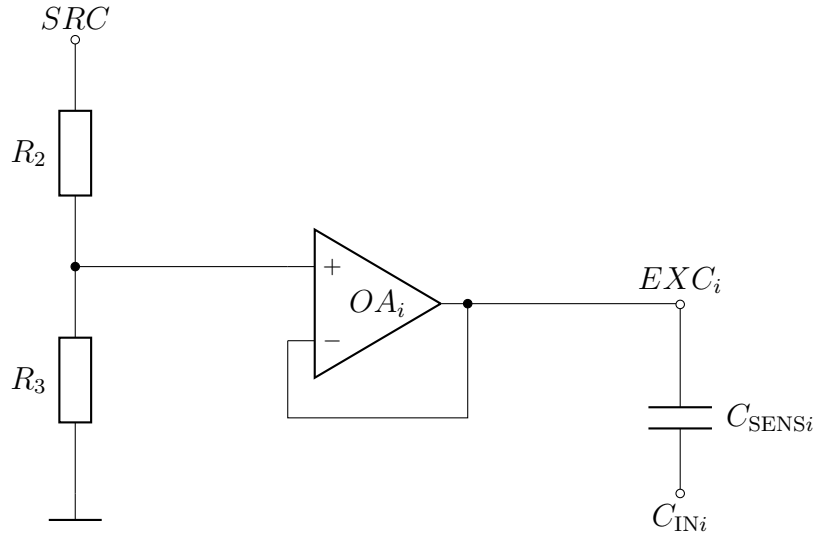
Figure 4.3: Capacitance input range extension circuit [16].

Our base value, determined in section 4.1 for a ice and snow free sensor is 143.994 pF and the maximum value for a water covered sensor is 357.052 pF. Thus the calculations are made for a maximum dynamic change of 220 pF. This results in a required range extension factor of

$$F \; = \; \frac{C_{\text{SENS,max}}}{C_{\text{IN,InputRange}}} \; = \; \frac{220 \text{ pF}}{4 \text{ pF}} \; = \; 55.$$

The factor F is the ratio between the excitation voltage V_{SCR} and the attenuated excitation signal V_{R3} at the positive input of the operational amplifier.

$$F \; = \; \frac{V_{\text{SCR}}}{V_{\text{R3}}} \; = \; \frac{R_2 \; + \; R_3}{R_3} \; = \; 1 \; + \; \frac{R_2}{R_3}$$

For R_2 we choose a value of 100 kΩ.

$$R_3 \; = \; \frac{R_1}{F \, - \, 1} \; = \; \frac{100 \cdot 10^3 \; \Omega}{55 \, - \, 1} \; = \; 1851.85 \; \Omega$$

With a value of 1820 Ω from E96 resistor table we get the following value for F.

$$F \; = \; 1 \, + \, \frac{R_2}{R_3} \; = \; 1 \, + \, \frac{100 \cdot 10^3 \; \Omega}{1820 \; \Omega} \; = \; 55.945$$

That leads us to the maximal measurable capacitance C_{DYN}.

$$C_{\mathrm{DYN}} \; = \; F \cdot C_{\mathrm{IN,InputRange}} \; = \; 55.945 \cdot 4 \; \mathrm{pF} \; = \; 223.78 \; \mathrm{pF}$$

For the calculated range extension factor F of 55.945, the circuit works just in a pretty low range. To extend the range F is increased to 233.558 by decreasing R_3 to 430 Ω. Although the circuit should be able to measure a capacitance of almost 1 nF, just the lower fifth is useable. This can be seen in figure 4.4 where the capacitance of one segment is set to zero (with the internal OFFSET register of the AD7143) and then equipped with different test capacitors C_{Test}. The value of the test capacitors C_{Test} are determined with a handheld LCR meter at 120 kHz. The relation between C_{Test} and C_{AD7143} is just for the three smallest values „linear". The first one with 74 pF represents an ice layer and the third one with 212 pF a water layer.

It seems the range extension circuit does not work accurate for such a high extension factors F. The circuit shown in [16] works with a factor of 12.
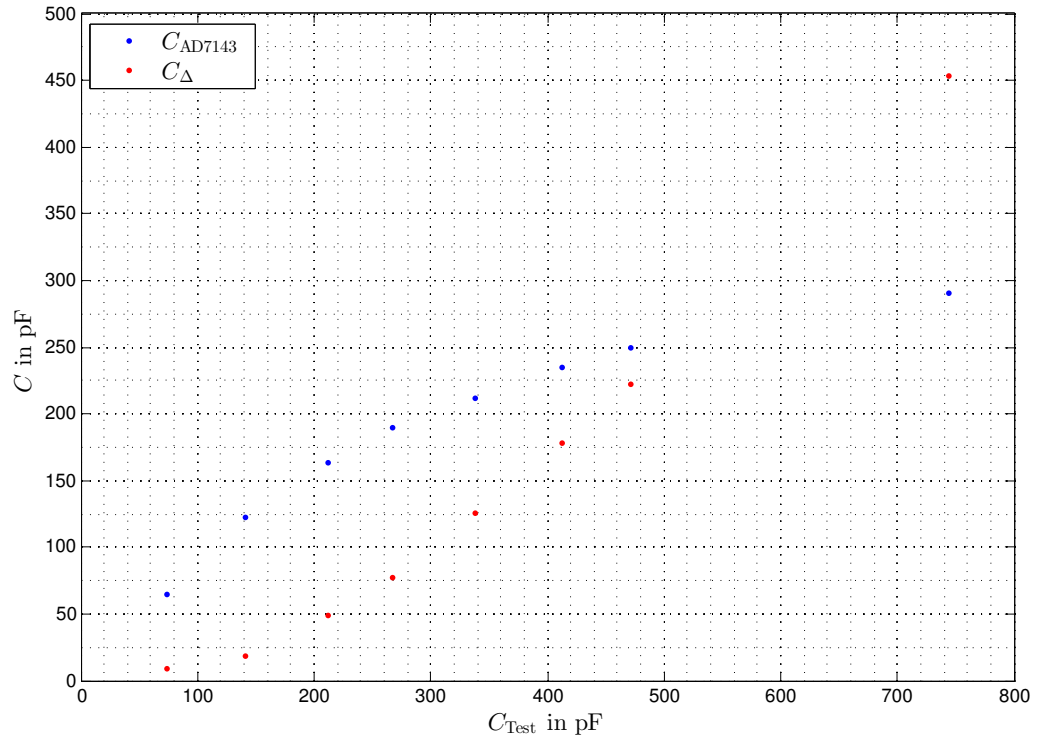
Figure 4.4: Measured capacitance C_{AD7143} of one sensor segment which is calibrated to 0 pF an equipped with C_{Test}. C_{Δ} is the difference between C_{AD7143} and C_{Test}.

4.3   Ice measurement

Several measurements are made to determine if the particular segments are covered
with ice. To freeze the heating unit (figure 3.17) the PCB is surrounded with a
copper sheet and the ventilation wholes are covered from the backside with tape,
as can be seen in figure 4.5. Because it is very tricky to remove the copper sheet
without detaching the ice layer from the heating unit, an additional measurement
is made before the copper sheet is removed. Three successful attempts are listed
in table 4.2, where C_{Cu} represents the results with copper sheet and C without.

Figure 4.5: Copper sheet surrounded sensor PCB with (blue) tape covered venti-
lation wholes, to freeze the PCB.

For the three successful attempts in table 4.2 it can be seen that the removing of the copper shield results in a small change of the capacitance. The difference of measurements can be explained by the undefined contact between PCB and ice. Thus it cannot be said which segment is completely iced. The only indication for a fully iced segment is the maximum value of about 140 pF for segment 3 at -10 °C. Furthermore the majority of the results are larger than expected by the FEM simulation. The frequency dependent permittivity ε_r of ice could be a reason for this mismatch. The capacitance measurement circuit operates at 250 kHz. There are no exact values available for this frequency. Therefore the electrostatic simulations are made with a ε_r of 3.2. This is a common value for frequencies larger than 100 kHz.

Temperature	-10 °C		-15 °C		-20 °C	
Segment	C_{Cu} in pF	C in pF	C_{Cu} in pF	C in pF	C_{Cu} in pF	C in pF
0	93.197	89.021	92.304	91.156	61.596	65.007
1	95.055	93.887	61.720	59.141	93.425	97.763
2	99.224	110.420	89.694	89.386	56.631	55.688
3	142.240	139.410	117.140	122.720	55.907	57.772
4	99.479	97.363	88.277	89.046	67.544	67.945
5	101.260	98.786	69.268	66.720	68.990	69.540
6	95.973	93.023	77.528	77.170	50.937	49.631
7	112.320	108.290	98.936	99.688	34.800	33.355

Table 4.2: Segment capacitance of the ice covered sensor - PCB at different temperatures.

A failed attempt is displayed in figure 4.6. Already such a tiny gap between ice layer and the PCB, with a thickness of 1.6 mm ends with a capacitance of 0 pF. Also the measurement of the failed de-icing attempt in figure 3.19 on page 29 results in a zero capacitance for each segment.

Figure 4.6: Gap between PCB (green) with a thickness of 1.6 mm and the ice layer that leads to a zero capacitance.

In figure 4.7 the variation of a water wetted segment is shown till everything is evaporated. The maximum value is 118.7 pF. Hence the capacitance of a partially wet segment is already in the range of a ice covered segment. This makes it complicated to detect ice around the freezing mark. That should not be a problem, because if the temperature determined by the meteorological sensor is below zero and the heating process starts, the water vaporises.
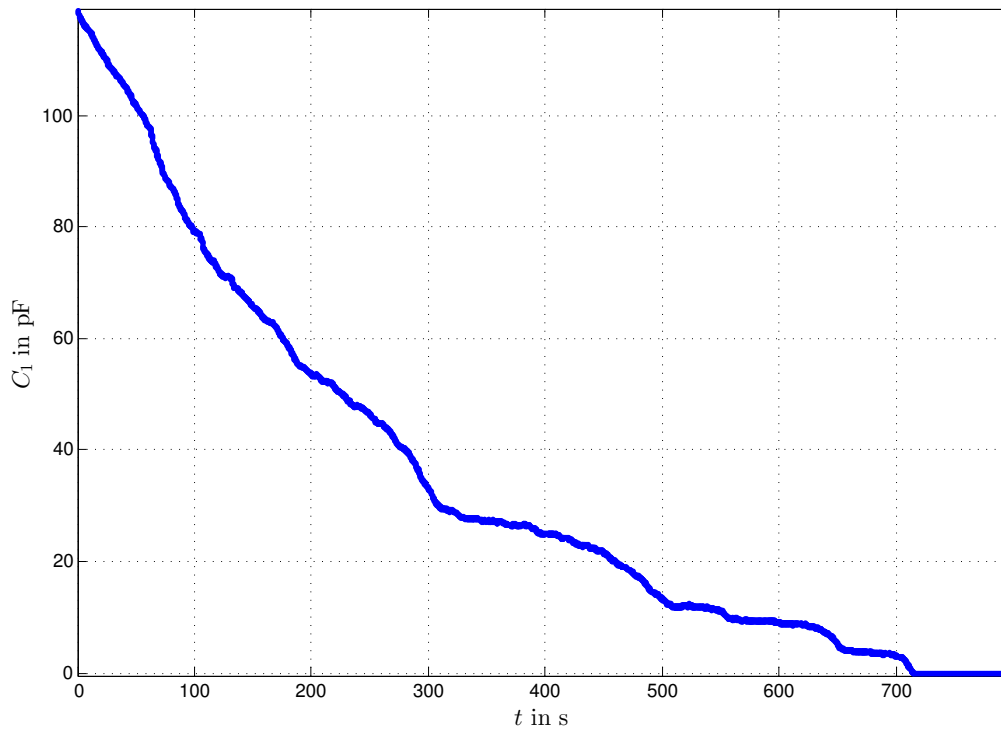
Figure 4.7: Variation of the water wetted segment number 1, till the whole water evaporates, at room temperature.
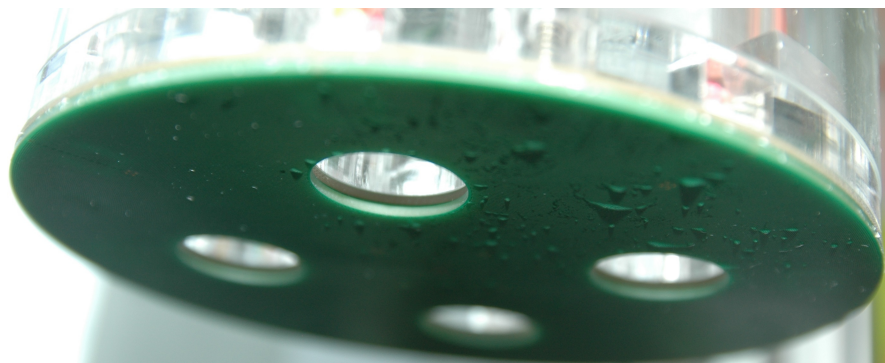
Figure 4.8: Water wetted segment number 1, at room temperature.

Surface temperature

As mentioned on page 45 it is very difficult to distinguish between an iced sensor segment and a wetted one. To facilitate the decision the surface temperature of the heating device is determined.

5.1 Temperature measurement with a constant current

Figure 5.1 shows how the existing circuit can be used to determine the surface temperature by adding a constant current source I_C and an optical relay S_{OPT} as well as by using one of the ADC inputs of the microcontroller. The optical relay (Omron G3VM-41HR) is used because it has a very low typical resistance of 0.03 Ω and a load voltage of 40 V. By turning off the PWM and switching the mechanical relays into the heating position, the voltage drop across the heating unit, caused by I_C, can be determined. With a temperature stable constant current source (LT3092) the resistance of the heating segments can be calculated. With equation 5.1 the temperature of the copper trace can be determined. The temperature coefficient α_{20} of copper at 20 °C is 3.9 $\cdot 10^{-3}$ K^{-1}. It should be mentioned that for very precise calculations the temperature coefficient itself is also slightly temperature dependent [17, page 421, 659].

$$T_{Surface} = \left(\frac{R_H(T)}{R_{20}} - 1 \right) \cdot \frac{1}{\alpha_{20}} + 20\ °C \qquad (5.1)$$

Unfortunately the protection circuit of the ADC has been damaged during the experiments. This results in a too large variation of the resistance which corresponds to a change of several degrees. To verify that the variation is not caused by another part of the circuit several different currents are supplied. The results are listed in table 5.1. It can be seen that the measurement principle works, even for a small current. Between each attempt the switch position of the mechanical relays are changed, to exclude a resistance variation caused by the relay contacts.
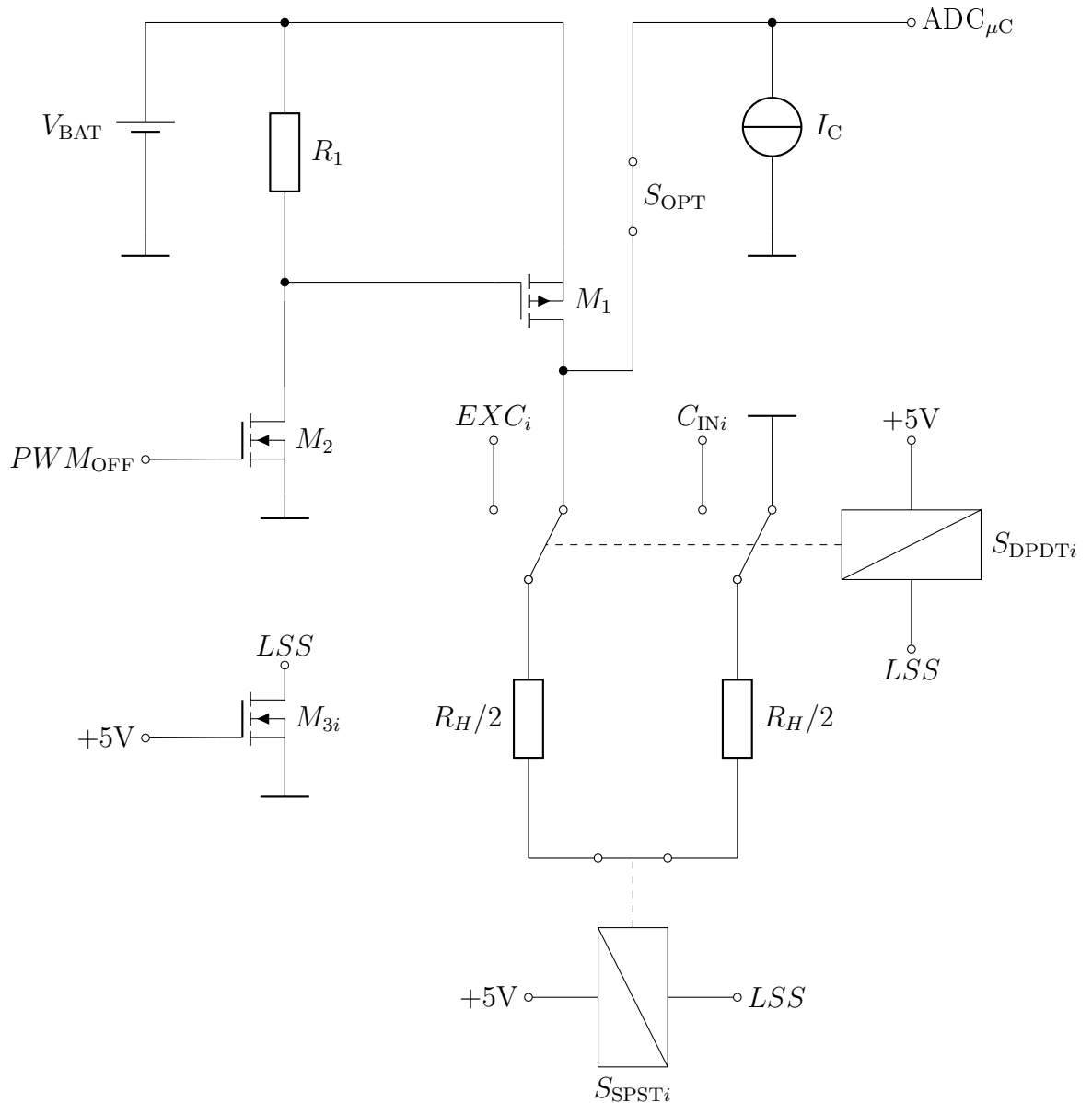
Figure 5.1: Circuit extension with I_C and S_OPT to determine the surface temperature of the heating segments.

Attempt	1			2			3		
Segment	V in mV	I in mA	R in Ω	V in mV	I in mA	R in Ω	V in mV	I in mA	R in Ω
0	351.5	9.95	35.327	351	9.94	35.312	350.9	9.94	35.302
1	362	9.91	36.529	361.6	9.9	36.525	361.5	9.9	36.515
2	338.5	9.98	33.918	338.2	9.98	33.888	338.1	9.98	33.878
3	320.2	10.04	31.892	320	10.04	31.873	319.9	10.04	31.863
0 ∥ 1 ∥ 2 ∥ 3	96.9	10.76	9.006	96.9	10.76	9.006	96.9	10.76	9.006
0	187.1	5.28	35.437	187.1	5.28	35.436	187	5.28	35.417
1	193	5.27	36.622	193	5.27	36.622	192.9	5.27	36.603
2	179.9	5.29	34.008	179.9	5.29	34.001	179.8	5.29	33.989
3	169.8	5.31	31.977	169.7	5.31	31.957	169.7	5.31	31.959
0 ∥ 1 ∥ 2 ∥ 3	50.6	5.5	9.2	50.6	5.5	9.2	50.6	5.5	9.2
0	97.1	2.72	35.699	97.1	2.72	35.699	97.1	2.72	35.699
1	100.3	2.72	36.875	100.2	2.72	36.838	100.3	2.72	36.875
2	93.3	2.73	34.176	93.3	2.73	34.178	93.3	2.73	34.176
3	87.9	2.73	32.198	87.9	2.73	32.198	87.9	2.73	32.198
0 ∥ 1 ∥ 2 ∥ 3	26.6	2.78	9.568	26.6	2.78	9.568	26.6	2.78	9.568

Table 5.1: Resistance of four separate segments and all four parallel. Between each attempt the switch position of the mechanical relays are changed. For the same current, the resistance of all three attempts is almost equal.

5.2 Temperature measurement with thermocouples

A second option to determine the surface temperature is implemented. Therefore, fine diameter thermocouples are mounted on the heating surface, which have a very small mass. Thus the heating process should not be distorted and no unheated spots should exist. This thermocouples are wired to ADCs with an internal amplifier on the STACK - PCB which is on top of the HEATING - PCB. To calculate the temperature the cold junction temperature T_{cj} is needed which is determined with an digital temperature sensor in the middle of the STACK - PCB.
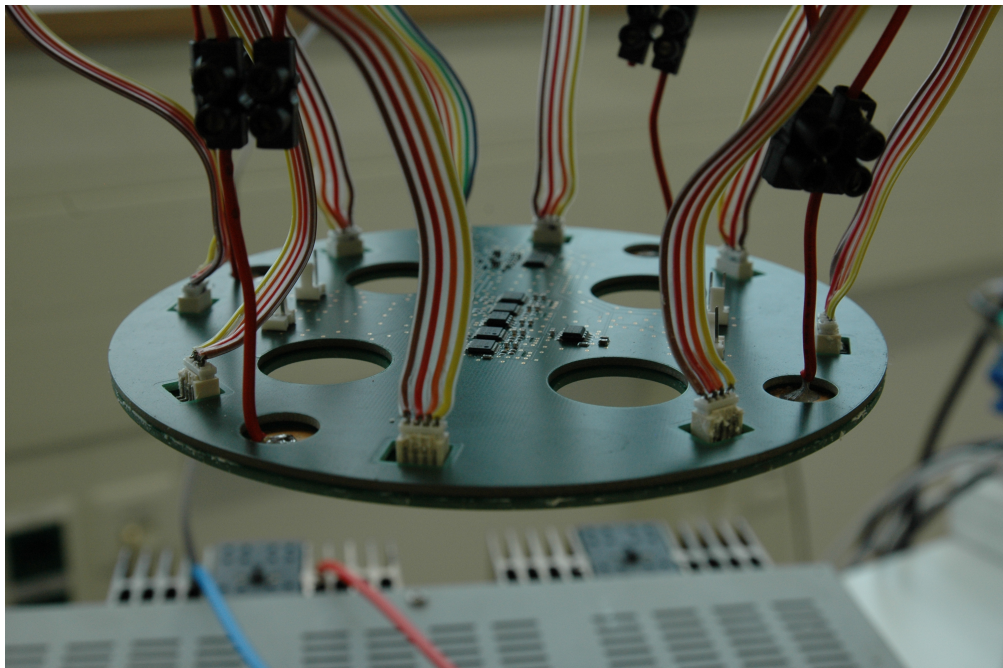
Figure 5.2: STACK - PCB on top of the HEATING - PCB, with the cold junction temperature chip in the middle of the five beaded one (surrounded by the four ADCs).

For each segment two thermocouples are used. This makes it possible to observe the temperature in a specific area. As it is shown in section 3.3 on page 18 the side of the heating unit which is facing the wind is colder than the side facing away. So the thermocouples can be used to determine the wind direction. This is important to ensure that just the segments are heated which are facing away from the wind. Otherwise the meteorological temperature measurement would be distorted by the intake of warmth air.

CHAPTER 6

Conclusion and further tasks

The developed and constructed weather and radiation shield shows that it is possible to keep the housing partially free of ice as desired. The de-icing attempts for natural convection established how critical non heated parts are and how they affect the de-icing process. The tests also show that the meteorological temperature is minimal distorted for short heating processes. Thus it can be said the main goal of the research is fulfilled.

For further investigations of the forced convection the more detailed *CFD* simulations have shown that two times more power is needed to keep the heating unit above 4 °C than determined by the simplified calculations. Thus a redesign of the heating unit should include wider copper traces to reduce the resistance of the segments. So a power supply with 24 V can be used. Furthermore attention should be paid on the covering of all VIAs with solder resist to avoid electrolysis. Using an alternating current to supply the heating unit would be an additional protection.

It has been shown that it is possible to integrate an ice detection device in the existing heating unit. Thus unheated spots can be minimized. The tests with an ice covered heating unit have shown that the ice can be detected. But the measurement results are highly influenced by the distance between ice and the sensor unit. Already a minimal gap leads to a zero capacitance. Thus for meaningful reference values it is necessary to make measurements with naturally grown ice. As expected it is very hard to distinguish between ice and water. This complicates the detection around the freezing point. The capacitance of a partially wetted segment is already in the scale of an ice covered one. The surface temperature of the heating unit may help to ease the decision.

As discussed it is possible to implement a surface temperature measurement with less layout effort. This approach bases on the temperature dependent resistance variation of the heating unit. A redesign of the CONTROL - PCB should include an external ADC with a high resolution. Thus a reliable measurement of the temperature dependent voltage drop across the heating segments, caused by the constant current source, is ensured. Nevertheless the thermocouples, which are not tested until now, have to be implemented. Because with the constant current source approach it is on the one hand not possible to heat the surface and on the other hand not to determine the temperature of the copper traces simultaneously. This could be reached by adding a TRMS - IC which records the heating current.

For forced convection tests a wind channel is needed. So the influence of the mentioned frustum on the fluid stream over the meteorological sensor can be tested as well as which dimensions do best fit. It should be possible to have a look into the housing during the measurements to observe a (colored) fluid stream. This wind channel should allow it to access the weather and radiation shield during the measurements from outside, to rotate the housing. Thus it can be tried if it is possible to detect the fluid direction with the thermocouples.

Bibliography

[1] Nordex SE. http://www.wind-lexikon.de/cms/v/ 174-vereisung.html. Online, accessed: 2013 March 25.

[2] Davis Instruments. http://www.davisnet.com/news/enews/ index.asp. Online, accessed: 2013 March 25.

[3] Rotronic AG. http://www.wittich.nl/EN/PDF/temhum/ weatherscreens/RS_Series.pdf. Online, accessed: 2013 March 21.

[4] Meteo Labor AG. http://www.meteolabor.ch/fileadmin/user_ upload/pdf/meteo/WX/vtp37_d.pdf. Online, accessed: 2013 March 22.

[5] G. Lufft Mess und Regeltechnik GmbH. http://www.lufft.com/ dateianzeige.php?Dateiname=/download/manual/8352_ USH4M_e.pdf. Online, accessed: 2013 March 21.

[6] Adolf Thies GmbH & Co. KG. http://www.thiesclima.com/wind_ glossary_e.html. Online, accessed: 2013 March 21.

[7] Ammonit Measurement GmbH. http://www.ammonit. com/images/stories/download-pdfs/DataSheets/ UltrasonicAnemometers/EN_DS_Ultrasonic_Thies_2D_40.pdf. Online, accessed: 2013 March 22.

[8] Ammonit Measurement GmbH. http://www.ammonit.com/images/ stories/download-pdfs/DataSheets/TemperatureHumidity/ EN_DS_Humidity-Temperature.pdf. Online, accessed: 2013 March 22.

[9] Rotronic AG. www.rotronic.co.uk/productattachments/index/ download?id=200. Online, accessed: 2013 March 22.

[10] Rotronic AG. www.rotronic.co.uk/productattachments/index/ download?id=299. Online, accessed: 2013 March 22.

[11] WeatherHawk. `http://www.weatherhawk.com/documents/` `600%20series%20instrument%20specifications.pdf` and `http://www.weatherhawk.com/documents/description%` `20weatherhawk%20600.pdf`. Online, accessed: 2013 March 22.

[12] Chem.-Ing. Rolf Kaltofen. *Tabellenbuch Chemie.* Wissenschaftlicher Verlag Harri Deutsch GmbH, 13. edition, 1998 (Frankfurt am Main).

[13] VDI-Gesellschaft Verfahrenstechnik und Chemieingenieurswesen. *VDI - Wärmeatlas.* Springer - Verlag, 10. edition, 2006 (Berlin, Heidelberg).

[14] Rudi Marek and Klaus Nitsche. *Praxis der Wärmeübertragung.* Carl Hanser Verlag, 3. edition, 2012 (München).

[15] Walter Frei. `http://www.comsol.com/blogs/` `which-turbulence-model-should-choose-cfd-application/`. Online, accessed: 2014 March 24.

[16] ANALOG DEVICES. `http://www.analog.com/static/` `imported-files/circuit_notes/CN0129.pdf`. Online, accessed: 2014 April 10.

[17] Horst Kuchling. *Taschenbuch der Physik.* Carl Hanser Verlag, 19. edition, 2007 (München).

54

Circuit diagrams

Serial interface

Socket with I2C - Bus and power supply for the STACK - PCB

I2C voltage level translator (3,3V and 5V)

Socket for the meteorological test sensors (MET - PCB)

Socket for the meteorological sensor

CONTROL - PCB
09.09.2014 13:01:50
Sheet: 1/5

Capacitance range extension
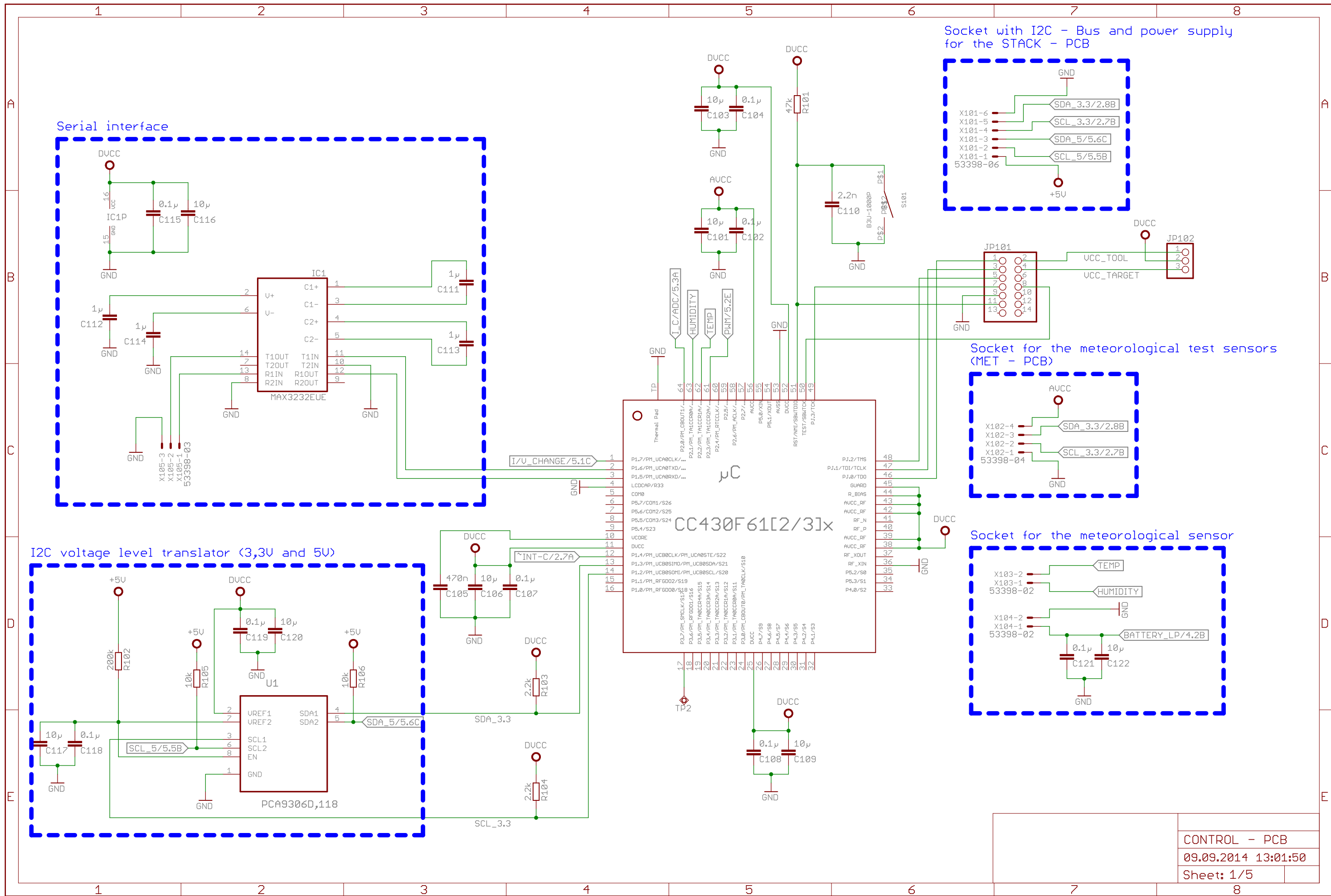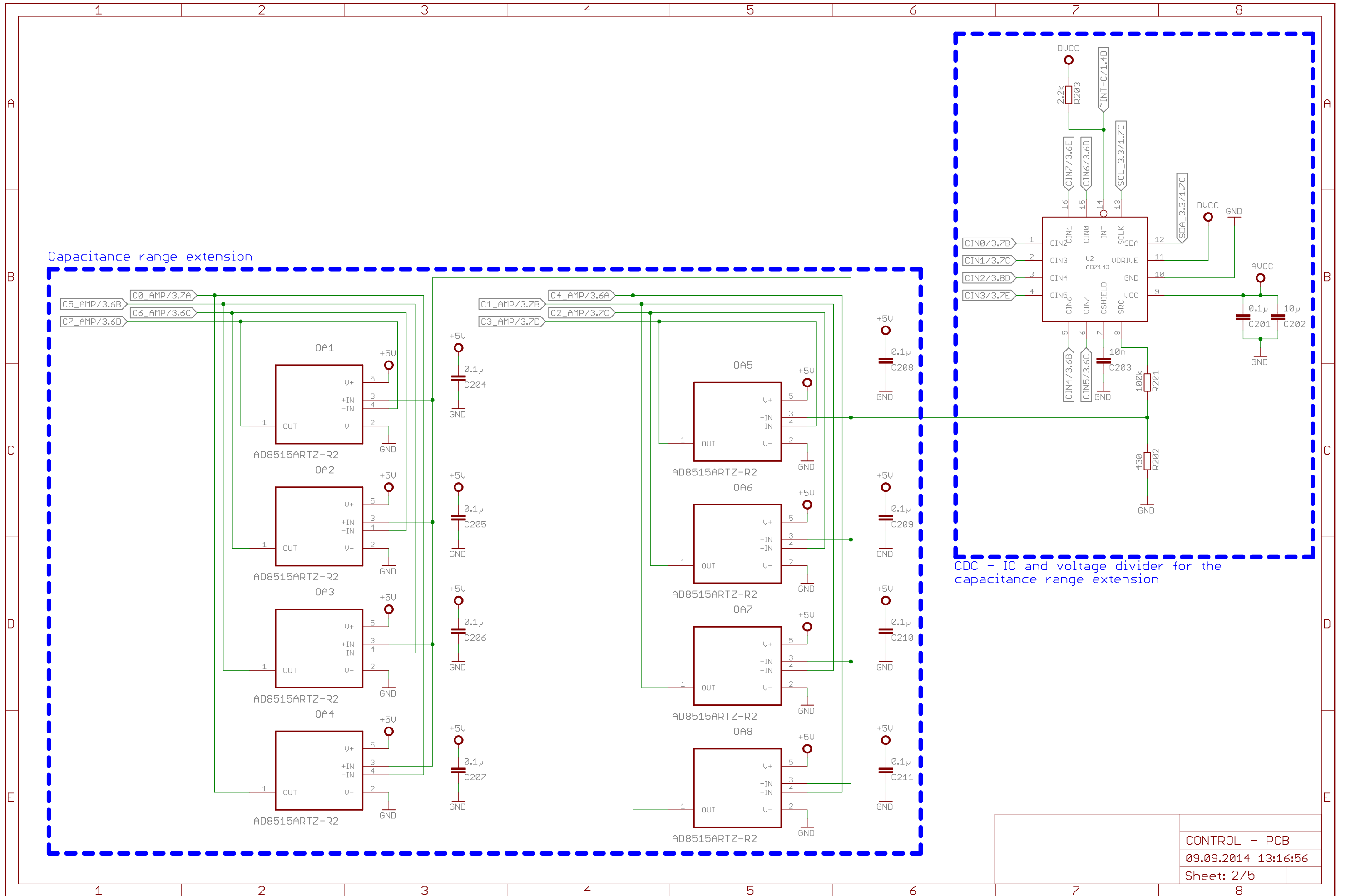
CDC – IC and voltage divider for the capacitance range extension

CDC IC (U2 AD7143):
- DVCC
- 2.2k R203
- INT-C/1.4D
- CIN7/3.6E
- CIN6/3.6D
- SCL_3.3/1.7C
- SDA_3.3/1.7C
- DVCC
- GND
- CIN0/3.7B — 1 — CIN2 — CIN1 — 16
- CIN1/3.7C — 2 — CIN3 — CIN0 — 15
- CIN2/3.8D — 3 — CIN4 — INT — 14
- CIN3/3.7E — 4 — CIN5 — SCLK — 13
- CIN6 — CIN7 — CSHIELD — SRC — 5 6 7 8
- SSDA — 12
- VDRIVE — 11
- GND — 10
- VCC — 9
- U2 AD7143
- CIN4/3.6B — 5
- CIN5/3.6C — 6
- 10n C203
- 100k R201
- AVCC
- 0.1µ C201
- 10µ C202
- GND
- GND
- 430 R202
- GND

Operational amplifiers (left):
- C5_AMP/3.6B
- C7_AMP/3.6D
- C0_AMP/3.7A
- C6_AMP/3.6C
- OA1 AD8515ARTZ-R2 — V+ 5, +IN 3, −IN 4, OUT 1, V− 2, GND — +5V, 0.1µ C204, GND
- OA2 AD8515ARTZ-R2 — V+ 5, +IN 3, −IN 4, OUT 1, V− 2, GND — +5V, 0.1µ C205, GND
- OA3 AD8515ARTZ-R2 — V+ 5, +IN 3, −IN 4, OUT 1, V− 2, GND — +5V, 0.1µ C206, GND
- OA4 AD8515ARTZ-R2 — V+ 5, +IN 3, −IN 4, OUT 1, V− 2, GND — +5V, 0.1µ C207, GND

Operational amplifiers (right):
- C1_AMP/3.7B
- C3_AMP/3.7D
- C4_AMP/3.6A
- C2_AMP/3.7C
- OA5 AD8515ARTZ-R2 — V+ 5, +IN 3, −IN 4, OUT 1, V− 2, GND — +5V, 0.1µ C208, GND
- OA6 AD8515ARTZ-R2 — V+ 5, +IN 3, −IN 4, OUT 1, V− 2, GND — +5V, 0.1µ C209, GND
- OA7 AD8515ARTZ-R2 — V+ 5, +IN 3, −IN 4, OUT 1, V− 2, GND — +5V, 0.1µ C210, GND
- OA8 AD8515ARTZ-R2 — V+ 5, +IN 3, −IN 4, OUT 1, V− 2, GND — +5V, 0.1µ C211, GND

CONTROL – PCB
09.09.2014 13:16:56
Sheet: 2/5

Relays to close/open the meander structure of the heating segmants

Ralys to switch between heating and capacitance measurement
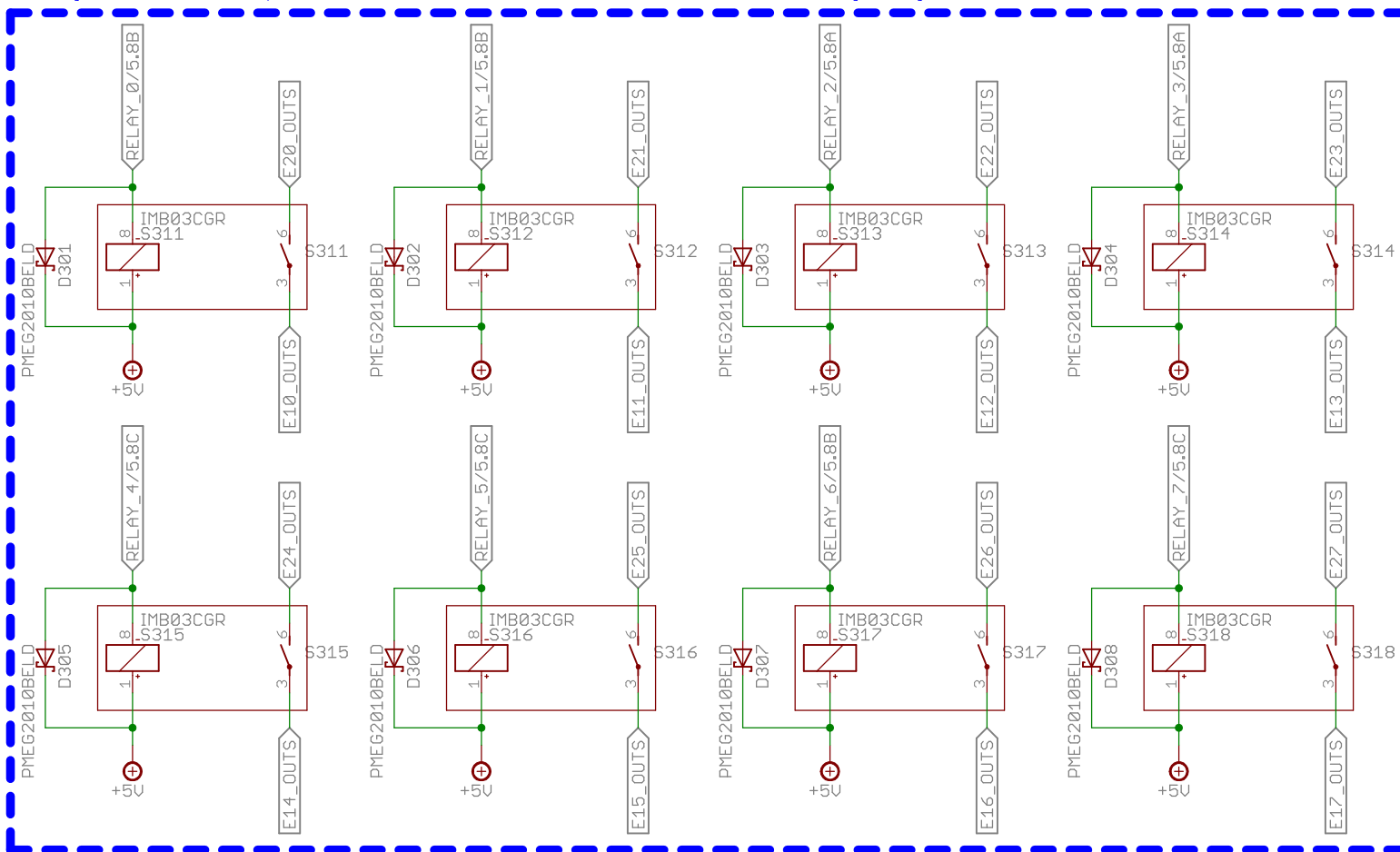
Sockets for the heating/sensor segments

CONTROL - PCB
09.09.2014 13:01:50
Sheet: 3/5
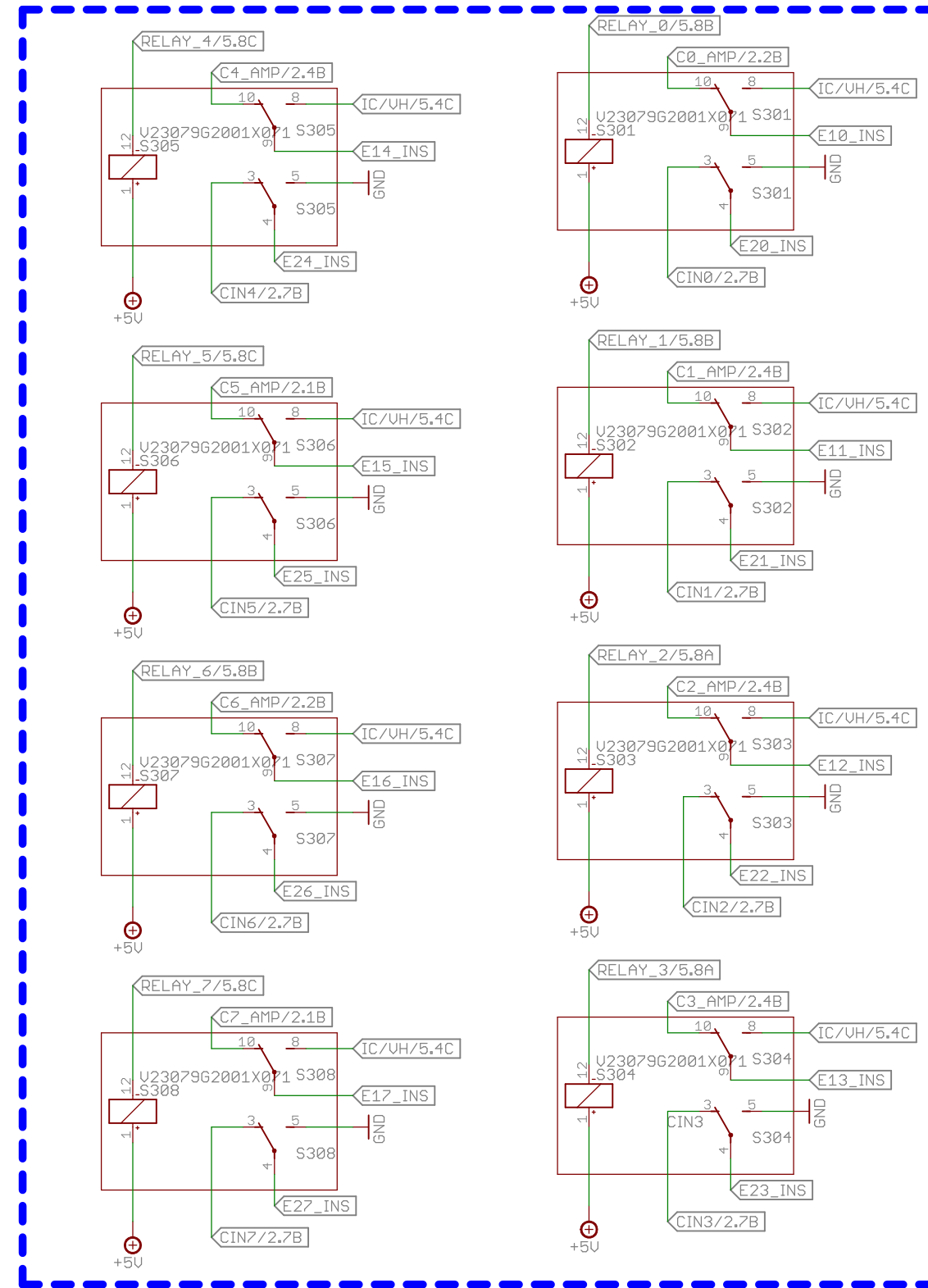
Buck -Converters:
V_in = 4,75V - 32V --> DVCC = 3,3V; 1A
V_in = 6,5V - 32V --> V_out = 5V; 1A

DCDC1
VIN GND VOUT
GND
P$2
R-78B5.0-1.0
P$1   P$3

DVCC

JP401
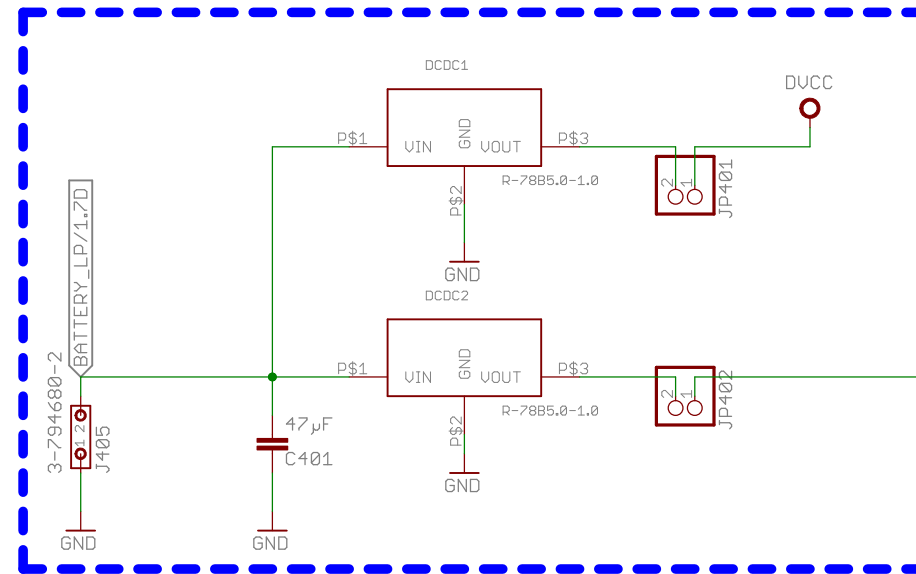
Anlalog reference voltage, AVCC = 3,3V; 100mA

DCDC2
VIN GND VOUT
GND
P$2
R-78B5.0-1.0
P$1   P$3

JP402

V-REF1
LT1461ACS8-2.5PBF

AVCC

BATTERY_LP/1.7D
3-794680-2
J405

47μF
C401

GND   GND

10μ
C404

0.1μ
C405

R401
100k

2 VIN   VOUT 6
3 ~SHDN
1 DNC_2
5 DNC_3
7 DNC_4
8 DNC
4 GND

10μ
C406

GND

GND
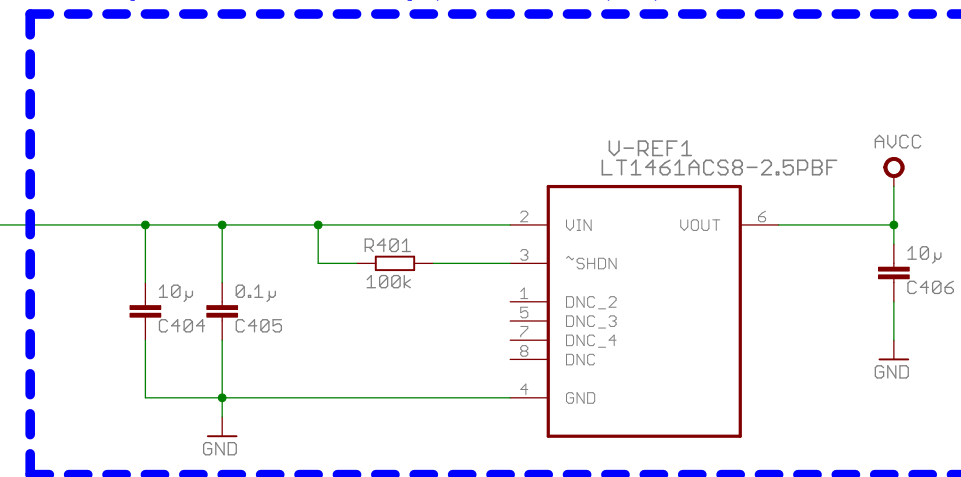
Buck - Converter:
V_in = 6,5V - 28V --> V_out = 5V; 4A

BATTERY_HP/5.5E

GND

J406
1 2

3-794680-4

DCDC3
R-745.0P

P$2*3 VIN   VOUT-ADJ P$12

P$1   ON/OFF   GND VOUT P$9*3

+5V

JP403

1μ
C402

P$5*4
GND

100μ
C403

GND   GND

CONTROL - PCB
09.09.2014 13:25:17
Sheet: 4/5

Constant current source I_c = 10 mA

AVCC

C501 1µ
C502 0.1µ
GND

R501 20k

I_CONST
7 IN_2
8 IN
5 SET
1 NC_2
2 NC

2 OUT_2
3 OUT_3
4 OUT

20 R523

LT3092ETS8TRPBF

JP501

I_C/ADC/1.5B
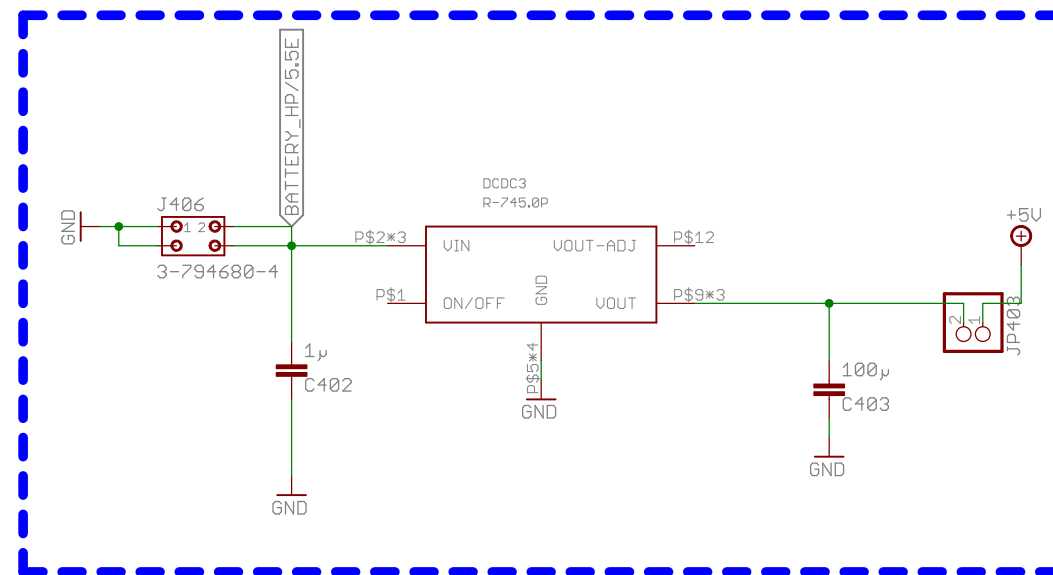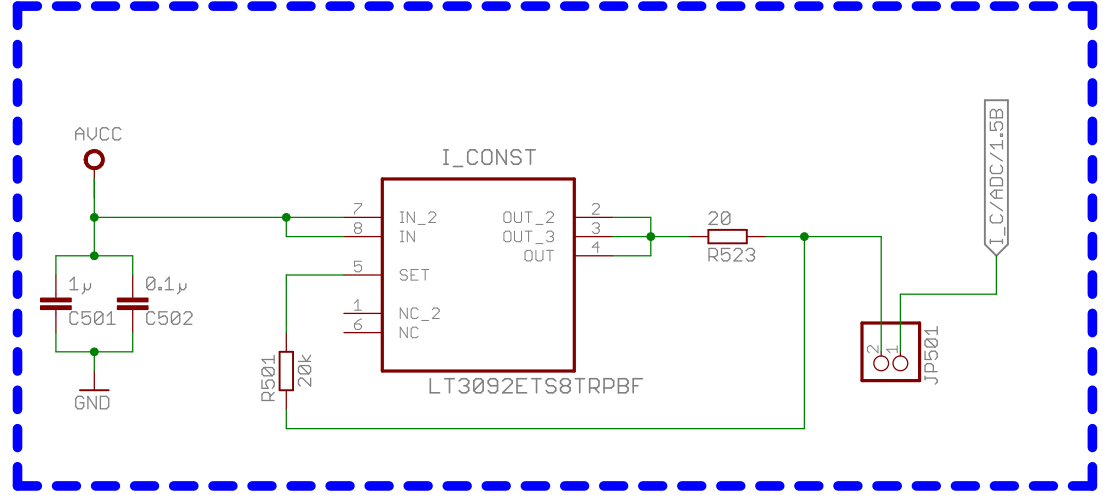
Optical relay to control the constant current source (typ. R_On = 30 mOhm)

+5V

T1
2 E
1 B
3 C

MMBT2369

GND

2.43k R503

I/V_CHANGE/1.4C

348 R502

S19
LED_A
LED_K
NC

DRAIN_6 6
SOURCE 5
DRAIN_4 4

G3VM-41HR

I_C/ADC/1.5B

IC/VH/3.8D
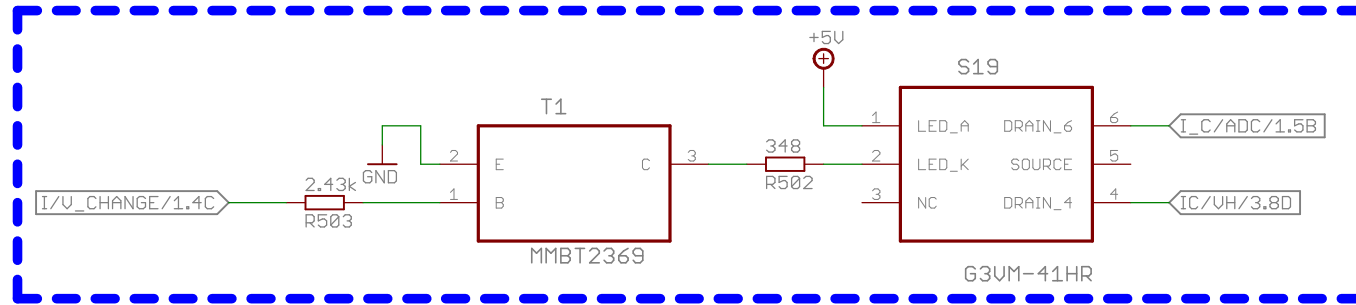
PWM with MOST – driver (MAX5048), N-MOST (NTR410N) to control the P-MOST (FDS6697)

+5V

C503 10µ
C504 1µ
GND

PWM/1.5B

TP1

1M R504

MD
1 V+
6 IN+
5 IN-
4 GND

P_OUT 2
N_OUT

MAX5048BAUT+T

GND

M2 NTR4170N

GND

M1

255k R505

IC/VH/3.8D

5 4
1 3

FDS6679

BATTERY_HP/4.3D
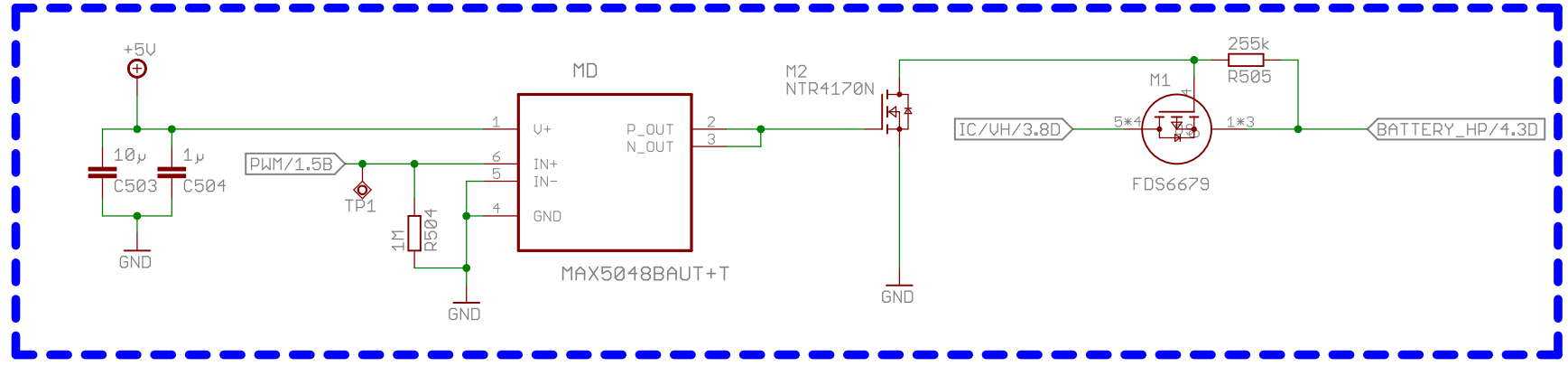
I2C controlled – switches and low side switchs to control the mechanical relays

+5V

C505 10µ
C506 0.1µ
GND

20k R506

GND

SWITCH-2
2 VDD
24 A0
22 A1
1 SCL
23 ~RESET
21 VSS
4 GND

S1 5
S2 7
S3 9
S4 11
S5 14
S6 16
S7 18
S8 20
D1 6
D2 8
D3 10
D4 12
D5 13
D6 15
D7 17
D8 19

SDA 3

ADG715BRUZ

SCL_5/1.7A

SDA_5/1.7A

+5V

R507 1k
R508 1k

R509 1k
R510 1k

R511 1k
R512 1k

R513 1k
R514 1k

47k R515
47k R516
GND GND

47k R517
47k R518
GND GND

47k R519
47k R520
GND GND

47k R521
47k R522
GND GND

GND

LS3
1 S1
4 S2
2 G1
5 G2
6 D1
3 D2

PMGD130UN

RELAY_2/3.7C
RELAY_3/3.7D

LS4
1 S1
4 S2
2 G1
5 G2
6 D1
3 D2

PMGD130UN

RELAY_0/3.7A
RELAY_1/3.7B

LS5
1 S1
4 S2
2 G1
5 G2
6 D1
3 D2

PMGD130UN

RELAY_6/3.6C
RELAY_7/3.6D

LS6
1 S1
4 S2
2 G1
5 G2
6 D1
3 D2

PMGD130UN

RELAY_4/3.6A
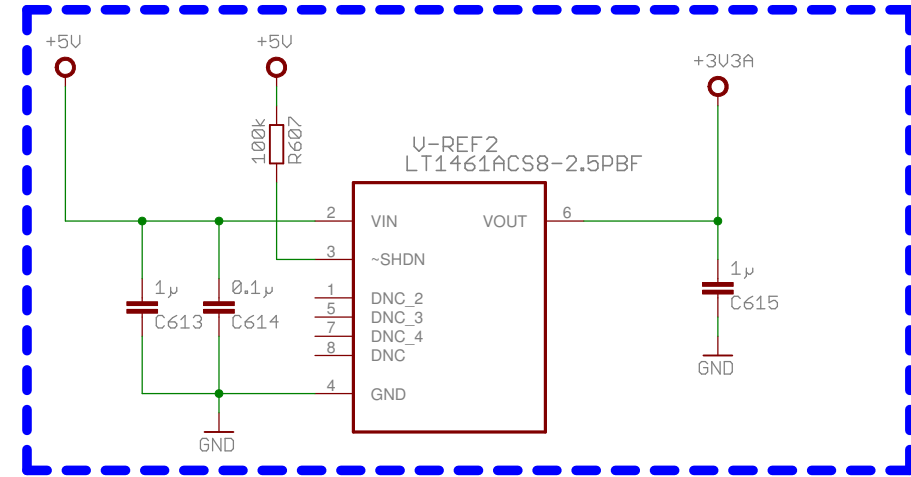RELAY_5/3.6B

CONTROL - PCB
09.09.2014 13:18:02
Sheet: 5/5

ADCs for the thermocouples
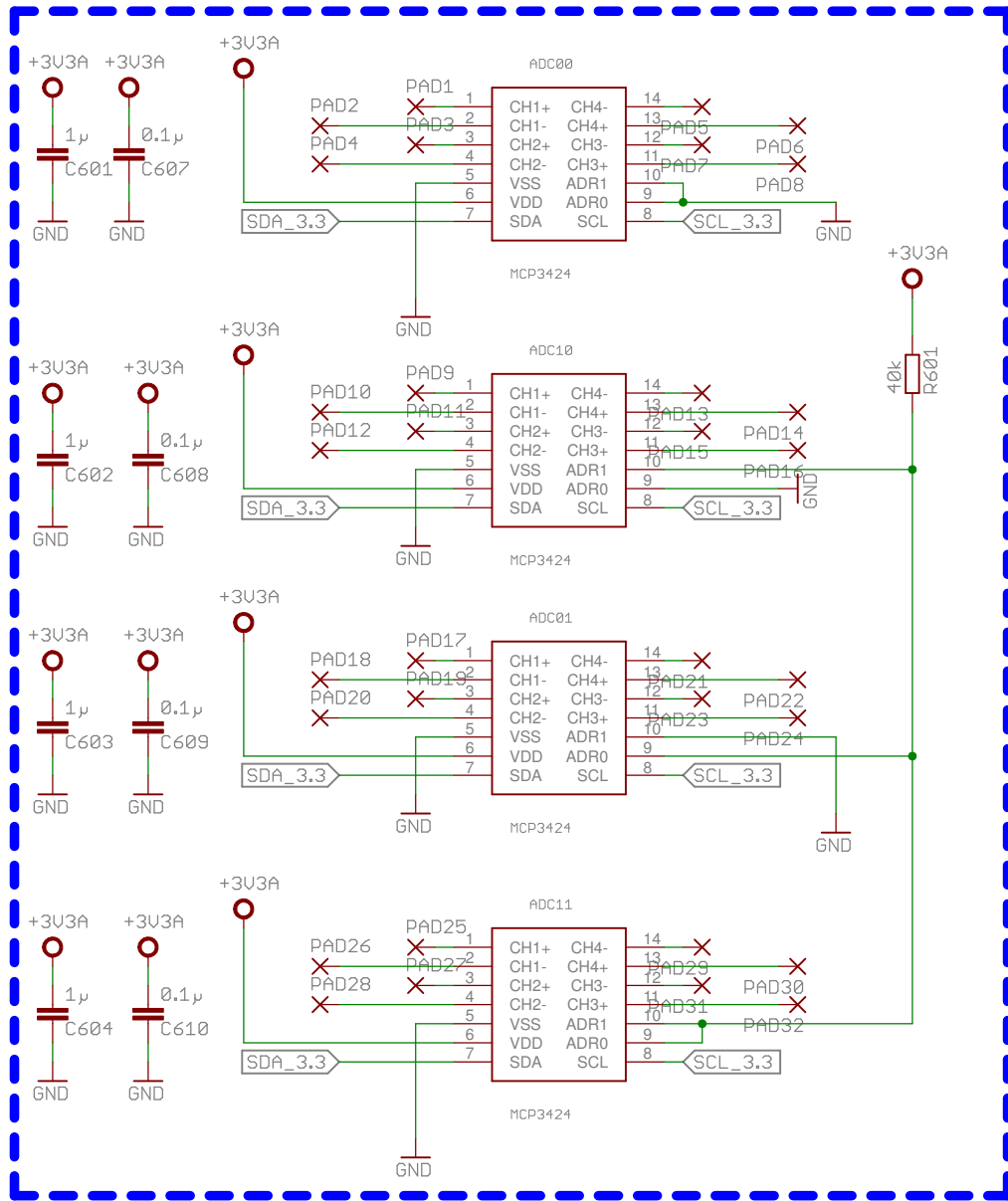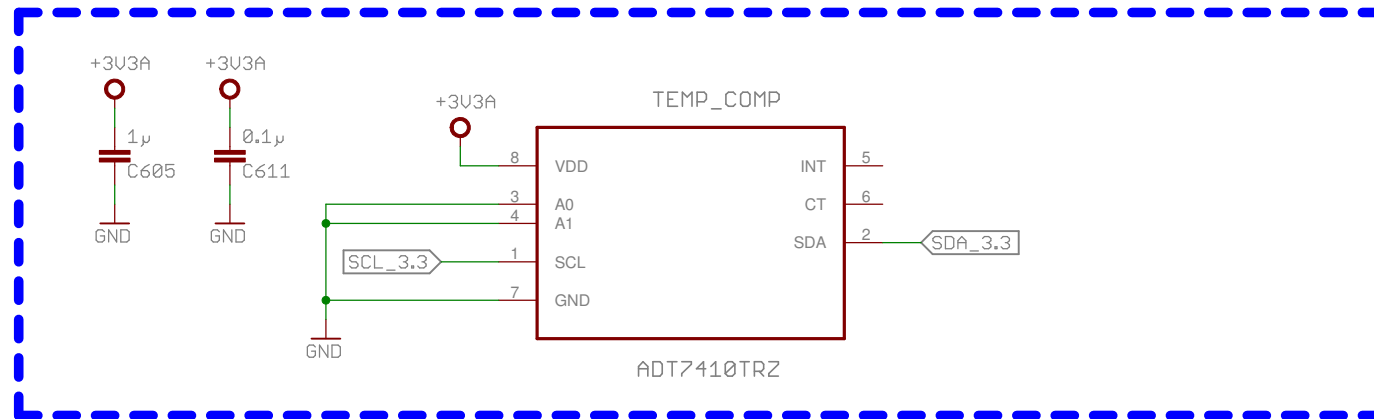
Fan control via I²C - Bus and Low Side Switchs
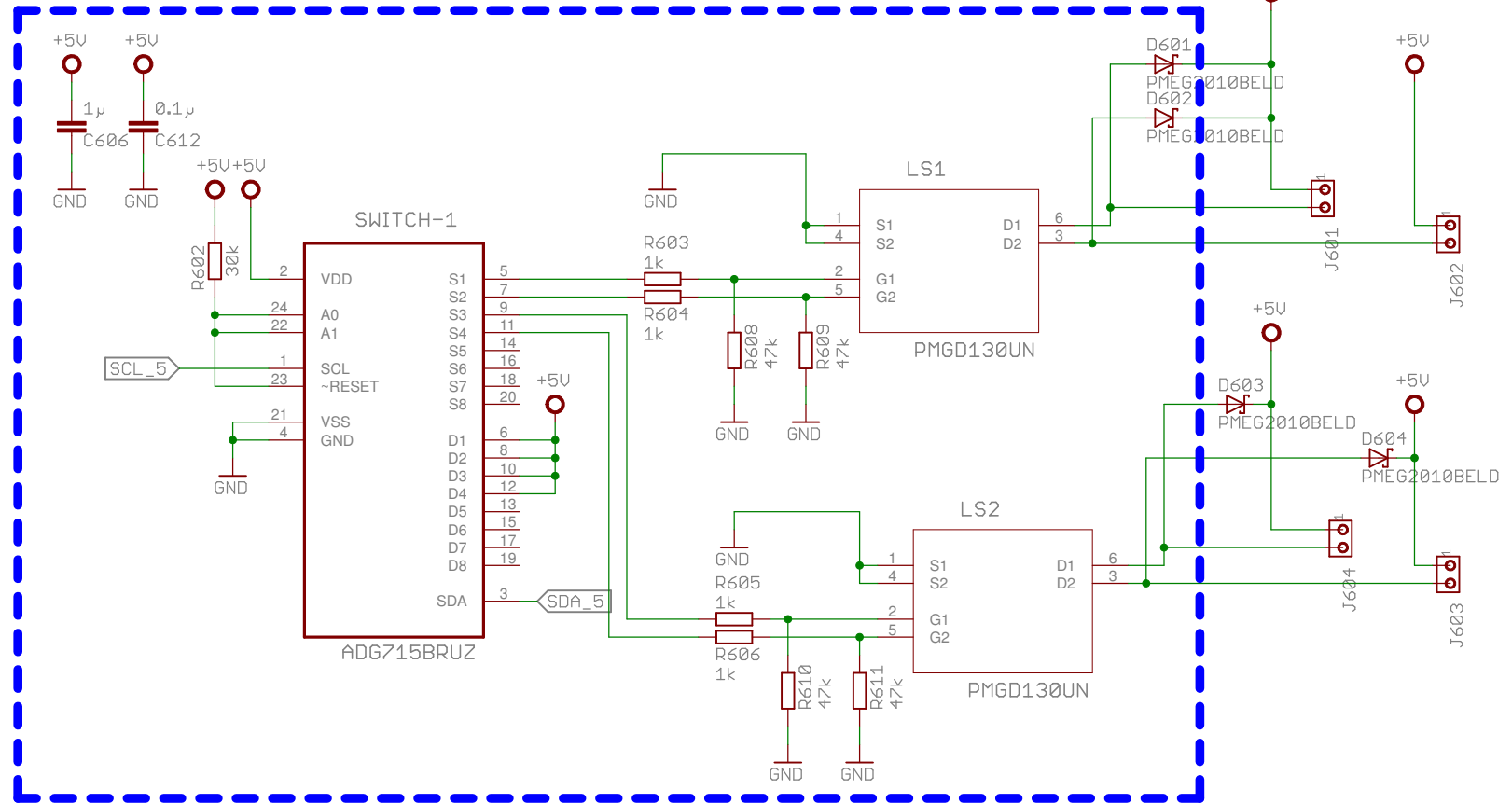
Voltage reference source, V_out = 3,3V; 100mA

Cold - temperature

Connection to the CONTROL - PCB

STACK - PCB
09.09.2014 13:21:29
Sheet: 1/1

HUMYDITY

SI7021

SDA_3.3 → 1 SDA SCL 6 → SCL_3.3
2 GND VDD 5
GND
3 DNC DNC1 4

DVCC

0.1µ
C701
GND

53398-04
X701-1
X701-2
X701-3
X701-4

DVCC

GND

SCL_3.3
SDA_3.3

TEMP-DUMMY

ADT7410TRZ

DVCC

10µ   0.1µ
C702   C703

10k
R701

GND

8 VDD   INT 5
3 A0   CT 6
4 A1
SCL_3.3 → 1 SCL   SDA 2 → SDA_3.3
7 GND

GND

MET - PCB

09.09.2014 13:27:32

Sheet: 1/1